

UC Davis

UC Davis Previously Published Works

Title

Quantifying Variability of Incipient-Motion Thresholds in Gravel-Bedded Rivers Using a Grain-Scale Force-Balance Model

Permalink

<https://escholarship.org/uc/item/6x61b295>

Journal

Journal of Geophysical Research Earth Surface, 128(9)

ISSN

2169-9003

Authors

Feehan, Scott A
McCoy, Scott W
Scheingross, Joel S
[et al.](#)

Publication Date

2023-09-01

DOI

10.1029/2023jf007162

Copyright Information

This work is made available under the terms of a Creative Commons Attribution License, available at <https://creativecommons.org/licenses/by/4.0/>

Peer reviewed

1 **Quantifying variability of incipient-motion thresholds in**
2 **gravel-bedded rivers using a grain-scale force-balance**
3 **model**

4 **Scott A. Feehan¹, Scott W. McCoy¹, Joel S. Scheingross¹, and Michael H.**
5 **Gardner²**

6 ¹Department of Geological Sciences and Engineering, University of Nevada, Reno, NV, USA
7 ²Department of Civil and Environmental Engineering, University of California, Davis, CA, USA

8 **Key Points:**

- 9 • Using a grain force-balance model and observed parameter distributions, we
10 quantify expected variability in incipient-motion thresholds
11 • Predicted distributions of incipient-motion thresholds match those observed in
12 laboratory experiments and natural rivers
13 • A power law can describe mean threshold of motion and its variability for the
14 relationship between grain size and threshold velocity

Corresponding author: Scott A. Feehan, sfeehan@nevada.unr.edu

Abstract

Predicting thresholds of sediment motion is critical for a range of applications involving sediment transport. However, thresholds for sediment motion can vary over an order of magnitude for a single characteristic flow and bed configuration. Lacking simple ways to incorporate this variability, many assume thresholds are constant for rough, turbulent flow. Here, we quantify variability of incipient-motion thresholds based on a commonly used grain-scale force-balance model, with model parameter distributions determined from published experiments. We show that variability in the threshold of motion within the 2D force-balance model occurs predominantly due to variability in the lift coefficient and grain protrusion, and secondarily due to drag coefficient variability. For a known grain size, the mean threshold of motion, and variability about the mean, can be predicted from a family of power laws. These power laws can be altered with site-specific parameter distributions, allowing for site-specific application to well-studied reaches and other planets. Using compiled flume and field data we show that constraining force-balance parameter distributions with independent data results in narrower distributions of the predicted threshold of motion, consistent with constrained flume experiments. This analysis highlights that while the threshold of sediment motion is variable, the magnitude of variability is predictable within the force-balance model based on site-specific physical constraints of local flow and bed conditions.

Plain Language Summary

Understanding what flow velocities are needed for rivers to move gravel and boulders is critical for river management, reducing flood hazards, understanding river ecosystems, and the long-term evolution of landforms such as deltas and mountain ranges. However, accurate predictions of sediment transport are made challenging by large variability in flow conditions observed when a particular size of sediment is moved by a river. In this work we use an existing theory to explore the expected flow conditions and flow variability needed to move sediment. These results allow for more accurate river restoration and engineering designs and more sustainable river management.

1 Introduction

When predicting sediment transport using popular empirical, deterministic approaches, a threshold of motion is required to define the condition below which sediment is static and above which sediment transport occurs (e.g., $\tau_c^* = 0.045$, where τ_c^* is the critical Shields stress for grain motion (Shields, 1936; Buffington & Montgomery, 1997)). This approach has been used in a variety of applications, including predicting the magnitude of bedload flux (e.g., Meyer-Peter & Müller, 1948; Fernandez Luque & Van Beek, 1976; Yager et al., 2007), understanding the hydraulic geometry of river channels (e.g., Parker, 1978; Pfeiffer et al., 2017; Phillips et al., 2022), modeling deposition, erosion, and subsequent evolution of river profiles (e.g., Parker, 1991; Wickert & Schildgen, 2019), predicting the occurrence of suitable habitat for aquatic organisms (e.g., Riebe et al., 2014; Wohl et al., 2015) and estimating the magnitude of past floods on Earth, Mars and other planetary bodies (e.g., Baker, 2002; Perron et al., 2006; Williams et al., 2013).

Many methods exist to estimate the threshold of motion. For example, the threshold can be quantified as a critical value of a non-dimensional parameter, such as τ_c^* , which roughly scales with the ratio of fluid stress on the grain to the grain weight, or as dimensional parameters such as the critical shear stress on the grain τ_c or a critical velocity near the grain u_c when motion first begins (Wiberg & Smith, 1987; Buffington & Montgomery, 1997; Garcia, 2008). Theory to predict these thresholds often use a

65 force-balance approach (e.g., Wiberg & Smith, 1987). In this case, motion is predicted
 66 to occur when the forces promoting grain motion (e.g., fluid drag and lift) exceed the
 67 forces resisting motion (e.g., the grain weight and friction). The force-balance method
 68 can predict threshold conditions for τ_c^* , τ_c , and u_c , and can be estimated using common
 69 field measurements (e.g., grain-size distribution and channel slope) combined with
 70 generalized assumptions about fluid drag. The ease of application of the force-balance
 71 method has led it to be perhaps the most commonly applied mechanistic method to
 72 predict the threshold of motion (e.g., Kirchner et al., 1990; Bridge & Bennett, 1992;
 73 Vollmer & Kleinhans, 2007; Recking, 2009; Scheingross et al., 2013; Prancevic et al.,
 74 2014; Lamb et al., 2017a; Yager, Schmeeckle, & Badoux, 2018).

75 However, not every underlying process that controls the onset of motion is captured
 76 in the force-balance framework. Recent work has demonstrated the importance
 77 of turbulent burst durations (known as impulse) (e.g., Diplas et al., 2008; Celik et
 78 al., 2013), moment and torque balances (e.g., Smart & Habersack, 2007; Lee & Bal-
 79 achandar, 2012; Dey & Ali, 2018), and the mechanism of grain entrainment (e.g.,
 80 establishing different criterion for initial particle motion via rolling, sliding or lifting of
 81 a grain out of its pocket) (Pähtz et al., 2020). These recently developed approaches re-
 82 quire more complex measurements to properly estimate the threshold of motion, such
 83 as estimating local inertial forces (e.g., Maniatis et al., 2020), high resolution flow tur-
 84 bulance data and/or a priori knowledge of the dominant entrainment mechanism (e.g.,
 85 Dey & Ali, 2017a). These requirements make these newly developed approaches more
 86 difficult to apply than the simple force balance, and hence the simple force balance,
 87 despite its shortcomings, remains in use. Furthermore, the force-balance approach is
 88 used and performs well in lab experiments, even when underlying model assumptions
 89 such as spherical grains, are broken (e.g., Prancevic & Lamb, 2015; Deal et al., 2023),
 90 and can explain a wide breadth of field and flume data (e.g., Lamb et al., 2008), where
 91 additional model assumption break down.

92 All of the above-mentioned methods to estimate the threshold of motion are
 93 deterministic; given known input parameters, the models output a single value for
 94 the threshold of motion. Field and flume data show there is not a single value for the
 95 onset of sediment motion, and instead, there is variability around a mean estimate. For
 96 example, in gravel-bedded rivers with slopes less than 5%, the critical Shields number
 97 is often estimated as $\tau_c^* \approx 0.045$, but experimental and field observations show that τ_c^*
 98 values can range from approximately 0.02 to 0.09 (Buffington & Montgomery, 1997).
 99 This variability may arise due to local differences in particle shape, flow characteristics,
 100 grain packing, style of initial motion (e.g., rolling vs sliding) and more (e.g., Kirchner
 101 et al., 1990; Hodge et al., 2013; Yager, Schmeeckle, & Badoux, 2018; Deal et al., 2023);
 102 but limited work to date (e.g. Lee & Balachandar, 2012) has shown how variations
 103 in these physical characteristics propagate through the force-balance model to set
 104 variability in observed incipient motion.

105 Here, we focus on estimating expected variability of the threshold of motion
 106 using the Wiberg and Smith (1987) force-balance model. While our analysis can be
 107 performed on other models (e.g., Dey & Ali, 2018; Pähtz et al., 2020), we explore the
 108 force-balance model because of its ease of application and common use. Furthermore,
 109 because the input parameters to the force-balance model are the most well constrained
 110 of any initial-motion model, using the force-balance model allows us to best explore how
 111 variability in model input parameters results in variability in the threshold of motion.
 112 In this sense, our goal is solely to describe expected variability within an existing model
 113 framework. While our work may yield insights on properties that control incipient
 114 motion within the force-balance model, we do not seek to fundamentally advance
 115 upon existing mechanistic descriptions of incipient motion.

116 Predicting the threshold of motion with the force-balance model requires several
 117 input parameters, which we refer to as force-balance parameters (FBPs). Variability

118 in turbulent fluid stresses, bed packing, grain exposure, and grain geometry result
 119 in FBP variability, and ultimately affect the threshold of motion (e.g., Shields, 1936;
 120 Grass, 1970; Gessler, 1971; Paintal, 1971; Kirchner et al., 1990; Church et al., 1998;
 121 Schmeeckle et al., 2007; Diplas et al., 2008; Booth et al., 2014; Lamb et al., 2017a;
 122 Yager, Schmeeckle, & Badoux, 2018; Masteller et al., 2019; Hassan et al., 2020). We
 123 hypothesize that a majority of the scatter in the threshold of motion observed in gravel-
 124 bed rivers is predictable and can be explained by expected FBP variability. Here, we
 125 quantify variability in the threshold of motion explicitly with expected distributions of
 126 critical velocity and critical shear stress at the onset of sediment motion. We do this
 127 by first quantifying the expected variability in each FBP using published laboratory
 128 experiments and detailed field studies, we then use a Monte Carlo method to propagate
 129 FBP variability through a deterministic force balance to estimate critical velocity and
 130 shear stress distributions at incipient motion. Constraining this variability allows us
 131 to quantify the expected variability in the threshold of motion, ultimately providing
 132 more robust, even if uncertain, sediment transport estimates.

133 2 Force-balance framework

134 2.1 Theoretical framework

135 Particle motion occurs when the forces promoting motion exceed the forces re-
 136 sisting motion (e.g., Wiberg & Smith, 1987). The forces promoting particle motion
 137 include the lift force, F_L , drag force, F_D , and the downslope component of the buoyant
 138 weight, calculated as $(F_G - F_B) \sin(\beta)$, where F_B is the buoyant force, F_G is the grav-
 139 itational force and β is the bed angle). We assume the buoyant force operates in the
 140 direction opposing the gravity vector and is vertical in our coordinate system (Wiberg
 141 & Smith, 1987; Chiew & Parker, 1995) rather than normal to the water surface as in
 142 Christensen (1995). The forces resisting motion, F_R , are the bed-normal component
 143 of the buoyant weight, F_N , and friction. The threshold of motion occurs when the
 144 forces promoting and resisting motion are balanced

$$F_D + (F_G - F_B) \sin(\beta) = F_R. \quad (1)$$

145 Following Wiberg and Smith (1987), we define the forces acting on the grain as

$$F_D = \frac{1}{2} C_D \rho A_e u^2 \quad (2)$$

$$F_L = \frac{1}{2} C_L \rho A_p u^2 \quad (3)$$

$$F_B = \rho g V_P \quad (4)$$

$$F_G = \rho_s g V_P \quad (5)$$

$$F_R = F_N \tan(\phi) = [(F_G - F_B) \cos(\beta) - F_L] \tan(\phi) \quad (6)$$

146 where g is gravitational acceleration, and ϕ is the effective friction angle that param-
 147 eterizes geometric and frictional resistance and is commonly written as the effective
 148 coefficient of friction $\mu = \tan(\phi)$. C_D and C_L are the effective drag and lift coefficients,
 149 respectively, ρ and ρ_s are the fluid and sediment densities, respectively and u is the

150 downstream flow velocity proximal to the grain (Schmeeckle et al., 2007). A_e is the
 151 upstream-facing cross-sectional area of the grain exposed to the flow. We calculate A_e
 152 assuming spherical grains as $A_e = A_n - A_b$, where $A_n = \pi r^2$ is the full upstream-facing
 153 cross-sectional area of the grain in the plane perpendicular to the mean bed surface,
 154 with r as the radius of the grain and A_b is the cross-sectional area of the grain that is
 155 buried or obscured from the flow, calculated as

$$A_b = r^2 \cos^{-1}((r - (D - p))/r) - (r - (D - p))\sqrt{2r(D - p) - (D - p)^2} \quad (7)$$

156 where p is the grain protrusion (defined as the height of the grain above the local mean
 157 bed elevation). A_p is the cross-sectional area of the grain in the plane parallel to the
 158 mean bed surface and is the area over which F_L is assumed to act. A_p is equivalent
 159 to the full cross-sectional area of the grain, A , when the relative protrusion value
 160 ($p_* = p/D$) is ≥ 0.5 . When $p_* < 0.5$, we calculate A_p as

$$A_p = \pi(r^2 - (r - p)^2) \quad (8)$$

161 (Figure 1a). These geometric definitions of A_e and A_p are dependent on the assumption
 162 of spherical grains with particle volume $V_p = 4/3\pi(D/2)^3$. We use the term
 163 ‘effective’ to describe parameters that depend on multiple factors, either owing to our
 164 use of simplified equations that neglect variably important physics, as in the case of
 165 F_D and F_L (Schmeeckle et al., 2007; Diplas et al., 2008; Celik et al., 2013; Dey et
 166 al., 2020), or are inherently formulated to include multiple contributing effects that
 167 are scale dependent, as in the case of ϕ (Booth et al., 2014; Yager, Schmeeckle, &
 168 Badoux, 2018). Similarly, because observations of ϕ and C_D are based on lab and
 169 field studies using natural grains mobilized via a mix of rolling and sliding, variability
 170 in observed distributions should capture the expected variability from the presence of
 171 non-spherical grains and different modes of initial motion. We use a 2D force balance
 172 to maintain consistency with previous work and we assume that the flow conditions
 173 at the time of entrainment are fully turbulent (Komar & Clemens, 1986; Lamb et al.,
 174 2008; Scheingross et al., 2013; Prancevic & Lamb, 2015; Ali & Dey, 2018). To avoid
 175 the complications of steep slopes and/or shallow flows on sediment mobilization, we
 176 further assume that the bed slope is constant at $\tan(\beta) = 10^{-3}$ and that grains are
 177 fully submerged within the flow.

178 We frame the threshold forces acting on the grain in terms of a critical grain-
 179 proximal velocity, u_c , by first substituting Equations (2) - (6) into Equation 1 to obtain
 180 an equality defining the critical state at initiation of motion

$$\frac{1}{2}C_D\rho A_e u_c^2 + (\rho_s g V_P - \rho g V_P) \sin(\beta) = ((\rho_s g V_P - \rho g V_P) \cos(\beta) - \frac{1}{2}C_L \rho A_p u_c^2) \tan(\phi) \quad (9)$$

181 and we rearrange Equation 9 to isolate u_c

$$u_c = \left(\frac{2(\rho_s/\rho - 1)gV_P (\cos(\beta) \tan(\phi) - \sin(\beta))}{C_D A_e + C_L A_p \tan(\phi)} \right)^{0.5}. \quad (10)$$

182 Equation 10 defines the grain-proximal downstream flow velocity that must be ex-
 183 ceeded to initiate sediment motion and is dependent on ρ , ρ_s , C_D , C_L , μ , and p (via
 184 A_e and A_p). Equation 10 does not explicitly account for turbulence; however, turbu-
 185 lence influences the value of C_D and C_L , allowing us to account for turbulence through
 186 including the large range of C_D and C_L values. The formulation of Equation 10, al-
 187 though often considered to represent a sliding entrainment mechanism, can be used to

188 represent flow conditions necessary for entrainment through other modes by altering
 189 the effective friction coefficient to approximate the frictional resistance appropriate
 190 for any given mode. For a rolling mode specifically, the effective friction coefficient
 191 is lower than that for a sliding mode (Kirchner et al., 1990). We use Equation 10
 192 to explore the influence of variability in the forces governing grain motion. We focus
 193 on the grain-scale critical velocity threshold, rather than reach-scale or time-averaged
 194 properties (e.g., reach-averaged shear stress or depth-averaged flow velocity), because
 195 near-bed fluctuations of flow velocity more accurately describe incipient motion than
 196 averaged flow measurements (Kirchner et al., 1990; Schmeeckle et al., 2007; Yager,
 197 Schmeeckle, & Badoux, 2018; Yager, Venditti, et al., 2018). Furthermore, using grain-
 198 scale velocity permits flow velocity estimates without requiring flow depth estimates.
 199 To aid comparison to existing data, we also cast the incipient motion threshold in
 200 terms of critical shear velocity, u_{*c} , critical shear stress and critical Shields stress in
 201 subsequent sections.

202 2.2 Variability of force-balance parameters

203 Estimating the variability in incipient motion using the force-balance framework
 204 described above requires quantifying the variability in the FBPs setting the threshold
 205 of motion. In this section we use published laboratory experiments and field surveys
 206 to develop the most general and broad FBP distributions that could be applicable
 207 in natural rivers of low slope (slopes $< 5\%$) with no additional information (e.g., no
 208 information on particle size or shape, water discharge, etc.). The distributions of
 209 force-balance parameters represent observed variability in space and time measured
 210 from independent experiments and field sites. As we show below, measured parameter
 211 variability is generally large relative to expected measurement uncertainty such that
 212 we assume distributions are dominated by observable variability, not measurement un-
 213 certainty. Furthermore, we assume that these limited observations have quantified the
 214 expected FBP variability. Many FBPs have documented parameter ranges, but lack
 215 quantified distribution forms. In these cases we assume parameters follow truncated
 216 normal distributions that have zero probability outside of specified ranges. These FBP
 217 distributions can be narrowed with additional site-specific or experiment-specific data
 218 (e.g., grain packing and particle density) as demonstrated in later sections.

Force-Balance Parameters						
Parameter Input	Drag C_D	Lift C_L	Friction μ (ϕ)	Relative Pro- trusion p_*	Fluid den- sity ρ (kg/m ³)	Sediment den- sity ρ_s (kg/m ³)
Mean	0.76	0.65	2.75 (70°)	0.7	1000	2650
Standard Deviation	0.29	0.29	0.27 (15°)	0.4	30	100
Minimum	0.1	0.06	0.27 (15°)	0.1	990	2500
Maximum	3	2	11.4 (85°)	1	1200	3000

Table 1. Values used to create generally applicable force-balance parameter distributions.

219 Grain and bed properties control the effective frictional resistance to motion
 220 (Yager, Schmeeckle, & Badoux, 2018). For a single grain in an idealized pocket geom-
 221 etry, the effective friction coefficient, $\mu = \tan(\phi)$, can be represented as the rotation
 222 angle between the grain being mobilized and the contact point with the downstream
 223 grain over which mobilization occurs (Figure 1a) (e.g., Wiberg & Smith, 1987). Nat-

224 ural bed sediments, however, are generally confined to pockets in which there are
 225 multiple points of contact and the grain may exit oblique to the downstream direc-
 226 tion, creating a distribution of μ values that can range from an effective angle (ϕ) of
 227 10 to 90 degrees (Kirchner et al., 1990; Hodge et al., 2013). Furthermore, μ is scale
 228 dependent such that the value for single-grain entrainment differs relative to sediment
 229 mobilization in force-chain clusters (Booth et al., 2014). Field, flume, and numerical
 230 studies commonly document log-normal μ distributions (Kirchner et al., 1990; Booth
 231 et al., 2014), with values likely resulting from variable importance of pocket geometry,
 232 grain shape and bed packing (Buffington & Montgomery, 1997; Johnston et al., 1998;
 233 Hodge et al., 2013; Prancevic & Lamb, 2015; Yager, Schmeeckle, & Badoux, 2018;
 234 Deal et al., 2023). We assume μ is log normally distributed around a mean effective
 235 friction angle of 70 degrees, a standard deviation of 15 degrees, and is truncated with a
 236 minimum and maximum of 15 degrees and 85 degrees, respectively (Table 1), which is
 237 representative of many naturally packed sediment beds (Hodge et al., 2013; Prancevic
 238 & Lamb, 2015).

239 The amount of grain protrusion p , adds additional variability as it modulates the
 240 grain area normal (A_e) and parallel (A_p) to the bed where F_D and F_L act, respectively
 241 (Kirchner et al., 1990; Yager, Schmeeckle, & Badoux, 2018). We use field observations
 242 to set the distribution of $p_* = p/D$; we assume p_* is normally distributed with a mean
 243 value of 0.7 (i.e., 70% of the grain height is exposed to the flow), and a standard
 244 deviation of 0.4 (Yager, Schmeeckle, & Badoux, 2018). We set the minimum p_* value
 245 to 0.1 based on field observations from Yager, Schmeeckle, and Badoux (2018) showing
 246 that >98% of non-buried grains have $p_* \geq$ to 0.1.

247 Fluid-grain interactions (as quantified in Equations 2 and 3) depend on effective
 248 drag and lift coefficients, C_D and C_L . C_D is commonly assumed to be dependent on
 249 grain size, grain shape, and particle Reynolds number, and is assumed to approach
 250 a value of 0.4 to 1 for natural channels (Ferguson & Church, 2004). However, near
 251 bed velocity fluctuations produce complex flow structures and changing points of flow
 252 separation under variable duration of the imposed fluid force, resulting in instantaneous
 253 C_D values deviating from the 0.4 - 1 range, even for constant grain size, shape and
 254 particle Reynolds number (e.g., Schmeeckle et al., 2007; Celik et al., 2013; Hurst et
 255 al., 2021). This variability in C_D is due to variably important physics, including form
 256 drag, skin friction and the effects of bed roughness, which are lumped into C_D within
 257 the simplified form of equation 2 (Lee & Balachandar, 2017; Dey & Ali, 2017a, 2017b;
 258 Li et al., 2019). Similarly, C_L , as represented in Equation 3, encompasses a wide array
 259 of processes including shear lift, Magnus lift, centrifugal lift, and turbulent lift that
 260 have uncertain relative influence on C_L (Ali & Dey, 2016; Dey et al., 2020). We assume
 261 both C_D and C_L follow a truncated normal distribution, with a mean C_D of 0.76 and
 262 range of 0.1 - 3, as measured for a spherical particle on a gravel bed in turbulent flow
 263 (Schmeeckle et al., 2007). Mean $C_L = 0.85C_D$ (Ali & Dey, 2016) and range from 0.06 -
 264 2. We assume a standard deviation of 0.29 for both C_D and C_L (Einstein & El-Samni,
 265 1949; James, 1990; Schmeeckle et al., 2007; Lamb et al., 2017a; Dey et al., 2020).

266 The remaining FBPs represent physical properties that, for a particular reach
 267 of interest, commonly have a narrow range. For generality, we assume the density
 268 of water varies from 0.99 g/cm³ to 1.2 g/cm³ (owing to variability in temperature or
 269 suspended sediment concentration) and that the density of grains varies with sediment
 270 lithology, from 2.5 g/cm³ for siliciclastic to 3.0 g/cm³ for mafic grains.

271 **2.3 Potential covariability of force-balance parameters**

272 All FBP distributions presented above are based on empirical observations. In
 273 this section, we account for the possibility that FBP values and distributions may co-
 274 vary. The most well established covariability between FBPs is for F_L and F_D , where

some represent F_L as the bed normal component of F_D at low slopes (Schmeeckle et al., 2007), while others have argued F_L is independent of F_D across a range of flow conditions (Celik et al., 2013). We assume that C_L and C_D are co-variable such that when sampling from FBP distributions (see Section 4), the same percentile value is selected from C_D and C_L given the parameter distributions described above. This relationship incorporates the observations that mean $C_L = 0.85C_D$ and that the effective strength of an imposed fluid force is the same relative magnitude in the downstream and vertical directions. We also explore a range of simplified linear relationships between C_L and C_D as a further test of other possible covariations (or lack of covariation) between C_L and C_D (Text S1 and Figure S1). Our results show that the magnitude of variability in the critical velocity for grain motion is only mildly sensitive to the amount of covariation (or lack of covariation) between C_L and C_D , with positive correlation between C_L and C_D resulting in higher critical velocities and negative correlation producing similar mean values as uncorrelated with reduced variability (Figure S1).

Covariance between the other FBPs has not been clearly established, however, relationships between FBPs may be inferred. For example, a high μ value may be correlated with a low p_* value for a grain sitting well below the mean height of surrounding grains (Yager, Schmeeckle, & Badoux, 2018). Complex bed structure precludes us from making these direct assumptions however, as a grain with a high μ may represent a grain that is fully exposed to upstream flow (p_* value near unity), but is sitting in front of a larger grain. Other FBPs have no clear correlation; for example, ρ and ρ_s have not been explored as co-variable in other FBP, and there is no physical reasoning that variance in particle or fluid density would dramatically influence bed packing via μ or alter C_D or C_L , given they are independent inputs to equation 2 and 3, respectively. Lacking established relationships between FBPs such as μ and p_* we rely on the FBP distributions as currently measured to ensure we represent all probable bed configurations in the general case explored here. We recognize that refining the probable relationships between all FBPs is a clear avenue for future work, the results of which could be incorporated into the proposed framework.

2.4 Influence of force duration

Grain-mobilization thresholds depend on the product of the magnitude of the force and the duration over which it is applied, a quantity termed impulse (Diplas et al., 2008; Pahtz et al., 2020). By systematically modulating imposed force duration and magnitude, Diplas et al. (2008) showed that the magnitude of critical force rapidly increased as the force duration became vanishingly small, which concentrated most of the observed variability in the threshold of motion towards exceedingly small duration of force application. For short force durations, forces well above critical are needed to rapidly accelerate and move the grain out of its pocket before the force pulse ends. However, subsequent work demonstrated that high magnitude, exceedingly short duration forces rarely mobilize grains (Celik et al., 2013). Instead, mobilization commonly occurs by longer force pulses sustained at or near the threshold force, where the threshold force is determined by accounting for all body and surface forces acting on the grain (Figure 1a).

We assume that the force that results from all sampled combinations of FBP values are applied with sufficient duration to mobilize the grain and thus correspond to a unique grain-proximal critical velocity capable of initializing grain motion. This assumption should not be limiting if grain mobilization is dominated by longer-duration near-critical forces, as has been demonstrated in highly controlled impulse experiments that have yielded FBPs consistent with the distributions used here (Schmeeckle et al., 2007; Celik et al., 2013; Maniatis et al., 2020).

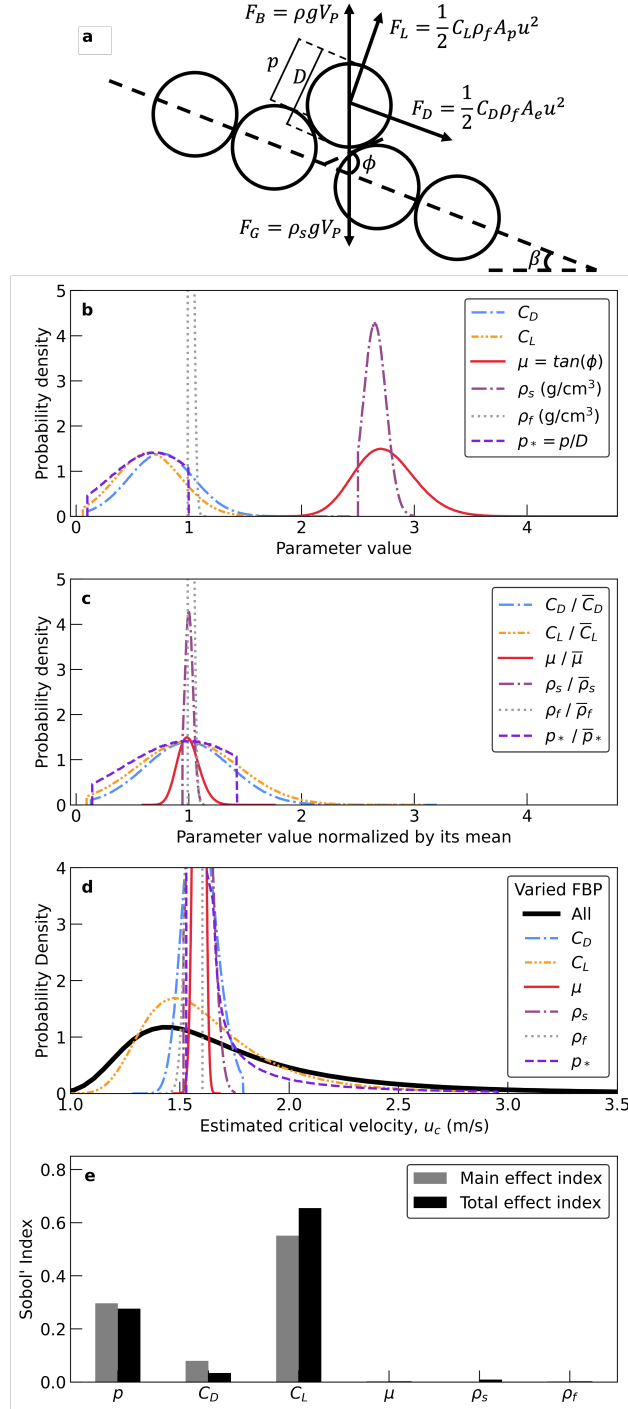


Figure 1. Variability of force-balance parameters (FBPs) and resulting sensitivity to these parameters. a) Schematic of forces acting on an individual grain (modified from Wiberg and Smith (1987)). b) FBP distributions for the general case given in Table 1. c) FBP distributions normalized by the mean value of each distribution. d) Estimated critical-velocity distributions for a 0.1 m diameter grain determined by varying all the parameters according to distributions shown in (a) (black solid line) compared to those resulting from varying each parameter individually while holding all others constant at their mean value (colored lines). e) Sobol' indices for each FBP indicating sensitivity of critical velocity to variability in FBPs. Light gray bars represent main effect indices and black bars represent total effect indices. In (b) - (d), y-axis limits truncate high-probability peaks of narrow distributions.

3 Sensitivity of critical velocity to variability in force-balance parameters

To determine which FBP distributions contribute most to the variability in incipient motion thresholds, we quantified the sensitivity of the expected critical velocity (Equation 10) to variability in each force-balance parameter using a one-at-a-time sensitivity analysis followed by a more formal global sensitivity analysis using Sobol' indices (Sobol, 2001). For the sensitivity analysis, we calculated the expected critical velocity distributions that resulted when only a single FBP was allowed to vary across its complete distribution, with all other FBPs held constant at their mean value. Sobol' global sensitivity indices provide estimates of the influence of individual or groups of variables on model outputs computed using Monte Carlo methods. We calculated Sobol' indices using Latin hypercube sampling and performed the global sensitivity analysis as implemented in the open-source software package `quoFEM` (McKenna et al., 2021). For this analysis, we used the distributions specified above (Figure 1b) and assumed near-perfect positive correlation between the lift and drag coefficients (correlation coefficient of 0.99). `quoFEM` allows users to wrap sensitivity analysis functionality around different analysis packages. In this case, we input a Python script describing the force-balance model as the input model for a global sensitivity analysis. We calculated both the main effect and total effect Sobol' indices to objectively assess the contributions of individual FBPs and FBP interactions to the overall variability in critical velocity predicted by our model. The main effect index provides a measure of an individual FBP's contribution to the total variance in the force-balance derived critical velocity, while the total effect index assesses variability added by a FBP due to its interaction with other FBPs.

For a given grain size, the one-at-a-time sensitivity analysis demonstrates that much of the observed variability in the critical velocity results from the lift coefficient and grain protrusion (Figure 1d) owing to the large variability of their distributions relative to their mean value (Figure 1c). This result does not indicate that other parameters such as μ and C_D are unimportant in setting the value of u_c ; instead, it suggests that the variability in the FBP distributions for parameters such as μ and C_D do not contribute substantial variance to the expected u_c distribution.

The global sensitivity analysis using Sobol' indices confirms a large individual contribution to the variability in critical velocity from the lift coefficient and protrusion value. The lift coefficient accounts for 58% of u_c variability, while the protrusion and drag coefficient account for 32% and 9%, respectively. Fluid and sediment density combined account for $< 1\%$ of the u_c variability. Similarly, the effective friction coefficient accounts for $< 1\%$ of the u_c variability (Figure 1d). The main effect and total effect for all FBPs show similar patterns, though the total effect is greater than the main effect in all instances. This indicates that interaction between FBPs contributes some amount to u_c variance, though C_L and protrusion dominate the variance, whether individually or through interactions with other FBPs. If grain size is allowed to vary and all other FBPs are assumed to be uniformly distributed, grain size alone accounts for 68% of the variability in u_c and reduces the main effect for C_L to 27%. This highlights that grain size is the most dominant independent variable for formulating an incipient motion threshold (Figure S1b). Using uniform distributions instead of truncated normal distributions for FBPs results in only minor changes in sensitivity (Figure S2a), suggesting that the relative contributions of FBPs to u_c variability is somewhat independent of the assumed form of the FBP distributions.

Although C_L , C_D , and p are rarely quantified and not well known in most environments, our analysis offers insight into their respective influence on the variability of incipient motion. This sensitivity analysis suggests that further constraints on effective lift, drag and protrusion would decrease expected variability in the threshold of motion. However, if such variability in FBPs is characteristic of a site where one

379 wants to predict sediment transport, then the large predicted variability is expected
 380 and should be used in incipient motion predictions.

381 **4 Model-predicted distributions of incipient motion thresholds**

382 To generate of critical-velocity distributions at incipient motion, we used a stan-
 383 dard Monte Carlo method to propagate FBP variability through Equation 10 (Metropolis
 384 & Ulam, 1949). We drew 10^5 random samples from each respective FBP distribution
 385 to solve Equation 10 for 10^5 unique realizations of critical velocity for a given grain
 386 diameter. We repeated this Monte Carlo procedure across 1000 grain sizes linearly
 387 spaced from 0.002 m to 1 m diameter and stacked the probability density functions of
 388 critical velocity determined for each grain size to create a probability density map of
 389 critical velocity that varied with grain size and represents the expected variability of
 390 the threshold of motion (Figure 2a).

391 To compare with other incipient-motion thresholds, we convert these grain-
 392 proximal velocities into corresponding critical shear velocities (u_{*c}), critical shear stress
 393 (τ_c), and critical Shields stress (τ_c^*) (Figure 2b-d). These conversions are not straight-
 394 forward, because u_c represents an instantaneous, point measurement, whereas u_{*c} , τ_c
 395 and τ_c^* are all spatially and temporally averaged quantities. However, given that u_* ,
 396 τ_b and τ^* are arguably the most commonly used metrics to evaluate the threshold of
 397 motion (e.g., Wiberg & Smith, 1987; Lamb et al., 2008; Garcia, 2008; Williams et
 398 al., 2013; Deal et al., 2023), being able to relate the variability we calculate in u_c to
 399 these averaged quantities represents a potentially useful contribution. Our approach
 400 is two-fold. We first assume that the instantaneous u_c value is approximately equal
 401 to the velocity averaged over the height of a grain, u_a , at incipient motion. Second,
 402 we take the full distribution of u_c values, and calculate a corresponding distribution
 403 of critical shear velocity using a known velocity profile as described below (Lamb et
 404 al., 2017b). This is similar to the approach of Wiberg and Smith (1987) in converting
 405 a local-scale grain velocity to critical shear velocity using a velocity profile; however,
 406 we make the additional assumption that the instantaneous u_c value can be treated as
 407 a time-averaged quantity solely for the purpose of calculating variability in u_{*c} . This
 408 should result in a wider distribution of critical shear velocity, consistent with our con-
 409 servative approach to estimate the maximum amount of variability in the threshold
 410 for motion. To convert to the corresponding u_{*c} , we also assume fully turbulent flow
 411 conditions such that the velocity profile is independent of Reynolds number and can
 412 be described by a modified logarithmic depth profile (Lamb et al., 2017b)

$$\frac{\bar{u}(z)}{u_*} = \frac{1}{k} \ln \left(1 + \frac{30z}{k_s} \right) \quad (11)$$

413 in which $\bar{u}(z)$ is the downstream velocity temporally averaged over turbulence and
 414 averaged laterally in space over variability in local bed roughness, z is distance above
 415 the bed, $k = 0.407$ is von Karman's constant, and k_s is the roughness layer height.
 416 From Equation 11 we calculate the velocity averaged over the height of a grain u_a . We
 417 assume that for a known grain size D , $u_a = u_c$ at incipient motion, given u_c represents
 418 the grain proximal downstream flow velocity in equation 10, we use this local velocity
 419 to solve for the corresponding u_{*c} , τ_c , and τ_c^* at incipient motion.

$$u_a = u_c = \frac{1}{z_2 - z_1} \int_{z_1}^{z_2} \bar{u}(z) dz = \frac{u_{*c}}{k(z_2 - z_1)} \int_{z_1}^{z_2} \ln \left(1 + \frac{30z}{k_s} \right) dz \quad (12)$$

$$u_c = \frac{u_{*c}}{(z_2 - z_1)k} \left(\left(\frac{k_s}{30} + z_2 \right) \ln \left(\frac{30z_2}{k_s} + 1 \right) - \left(\frac{k_s}{30} + z_1 \right) \ln \left(\frac{30z_1}{k_s} + 1 \right) - z_2 + z_1 \right) \quad (13)$$

$$u_{*c} = u_c(z_2 - z_1)k \left(\left(\frac{k_s}{30} + z_2 \right) \ln \left(\frac{30z_2}{k_s} + 1 \right) - \left(\frac{k_s}{30} + z_1 \right) \ln \left(\frac{30z_1}{k_s} + 1 \right) - z_2 + z_1 \right)^{-1} \quad (14)$$

420 where z_1 and z_2 represent the vertical position of the bottom and top of the grain of
421 interest, respectively.

422 We assume k_s ranges from $D \leq k_s \leq 6.1D$ and we allow the grain to sit anywhere
423 within the roughness layer, that is, $k_s/30 + D \leq z_2 \leq k_s$ and set $z_1 = z_2 - D$ (Grant,
424 1997; López & Barragán, 2008). While other work has suggested narrow ranges in
425 k_s (e.g., Lamb et al., 2017b), the large range used here ensures the widest possible
426 distribution of critical velocities, consistent with our goal to quantify the maximum
427 amount of potential variability in the force-balance approach.

428 For each Monte Carlo realization of Equation 10, we predicted the variability
429 of critical shear velocity by randomly sampling values of k_s and z_2 from uniform
430 distributions with limits as specified above, and we propagate those estimates through
431 Equation 14, (Figure 2b). Assuming a constant k_s (e.g., $k_s = D$) reduces the variability
432 by up to half relative to the case in which k_s varies within a uniform distribution
433 (Figure S4). We calculated the variability for critical shear stress and critical Shields
434 stress using

$$\tau_c = \rho u_{*c}^2 \quad (15)$$

435 and

$$\tau_c^* = \frac{\rho u_{*c}^2}{(\rho_s - \rho)gD} \quad (16)$$

436 The resulting distributions (Figure 2) highlight the expectation of large variability
437 in incipient-motion thresholds given the measured variability in FBPs, but also
438 show that well-defined high-density regions for each threshold can be characterized by
439 the interquartile range (IQR) (Figure 2). We found that these high-density regions in
440 the threshold u_c , u_{*c} , and τ_c distributions can be represented by a family of power
441 laws fit between grain size and the respective flow parameter, with u_c and u_{*c} different
442 only by their coefficient

$$u_c = m_c D^{0.5} \quad (17)$$

$$m_c = 5.21 \pm 0.91$$

$$u_{*c} = m_* D^{0.5} \quad (18)$$

$$m_* = 0.80 \pm 0.17.$$

445 These power laws are based on the form of Equation 10, in which the FBP distributions
446 reported in Table 1 result in a power law characterized by the reported m_c , while the
447 power law exponent of 0.5 remains fixed. We solve for the best fit of τ_c by combining
448 Equations 15 and 18, $\tau_c = \rho u_{*c}^2 = \rho m_*^2 (D^{0.5})^2$ which results in the linear relationship

$$\tau_c = m_\tau D \quad (19)$$

$$m_\tau = 648 \pm 285$$

450 where $m_\tau = \rho m_*^2$. Combining Equations 15, 16, and 19 yields $\tau_c^* = m_\tau / (\rho_s - \rho)g$,
451 resulting in a constant τ_c^* value of

$$\tau_c^* = 0.040 \pm 0.018. \quad (20)$$

452 These functional relationships shown in Equations 17, 18, 19 and 20 predict a wide
 453 range of incipient motion thresholds, owing to our use of broad FBP distributions
 454 (Table 1) and thus should be valid, albeit with large expected variability, for spherical
 455 grains on Earth in low slope rivers. As we show below, if additional site-specific infor-
 456 mation is available (e.g., known sediment density, or a known and tighter range of drag
 457 coefficients), input FBP distributions can be narrowed, resulting in reduced variability on
 458 the power law coefficients (m_c , m_* , m_τ) or τ_c^* estimate.

459 **5 Comparison between model-predicted and empirically-observed incipient-** 460 **motion thresholds and bedload flux**

461 In this section we compare incipient-motion distributions predicted by our model
 462 to published data from flume experiments with controlled and limited parameter vari-
 463 ability and field data with wider FBP ranges. We also use our model framework
 464 to show how variations in the incipient-motion threshold offer an explanation of the
 465 scatter in existing bedload flux measurements. These comparisons serve as concrete
 466 examples of how FBP distributions and resulting predictions of threshold distributions
 467 can be narrowed for a particular site of interest.

468 **5.1 Comparison with large-replicate, single-grain entrainment flume ex-** 469 **periments**

470 We compared our model-predicted critical velocity distributions with published
 471 distributions measured in idealized flume experiments. Wu and Shih (2012) replicated
 472 two experiments of grain-entrainment (115 and 205 replicates, respectively) by placing
 473 spherical grains in idealized pocket geometries and measuring grain proximal veloci-
 474 ties before and after initial grain motion using high-speed cameras and laser Doppler
 475 velocimetry. They found that the critical velocity at entrainment was not constant
 476 across replicates for an experiment, but instead took on a range of values well outside
 477 the uncertainty in their velocity measurements (Figure 3). The Wu and Shih (2012)
 478 experiments provide idealized data to test the accuracy of our force-balance model
 479 predictions in a fully controlled setting.

480 To compare our model predictions to the Wu and Shih (2012) data, we narrowed
 481 our input FBP distributions based on the experimental setup. We set the C_D distri-
 482 bution using the experimentally measured median velocity prior to entrainment based
 483 on the relationship between C_D and u_a measured by Schmeeckle et al. (2007) (Figure
 484 S3). Similarly, we decreased the mean and narrowed the range of μ to reflect the
 485 experimental pocket geometries and observed direction of initial sediment motion out
 486 of the pocket following Kirchner et al. (1990):

$$\mu = \tan(\phi) = \frac{\gamma}{\sqrt{(D_m/D_b)^2 + 2(D_m/D_b) - 1/3}} \quad (21)$$

487 where D_m is the diameter of the spherical particle being mobilized, D_b is the diameter
 488 of the spherical, uniform bed particles and γ is an empirical coefficient that is equal to
 489 $1/\sqrt{3}$ when the mobilizing particle pivots through the saddle between two downstream
 490 bed particles and is equal to $2/\sqrt{3}$ when the mobilizing particle pivots directly over
 491 one of the bed particles. This semi-empirical formulation uses a rolling initiation
 492 mechanism to calibrate the effective coefficient of friction. Although our balance of
 493 forces in Equation 1 is not based on a moment balance in which the rolling regime of
 494 particles are defined (e.g., Pähtz et al., 2020), Equation 21 allows us to characterize

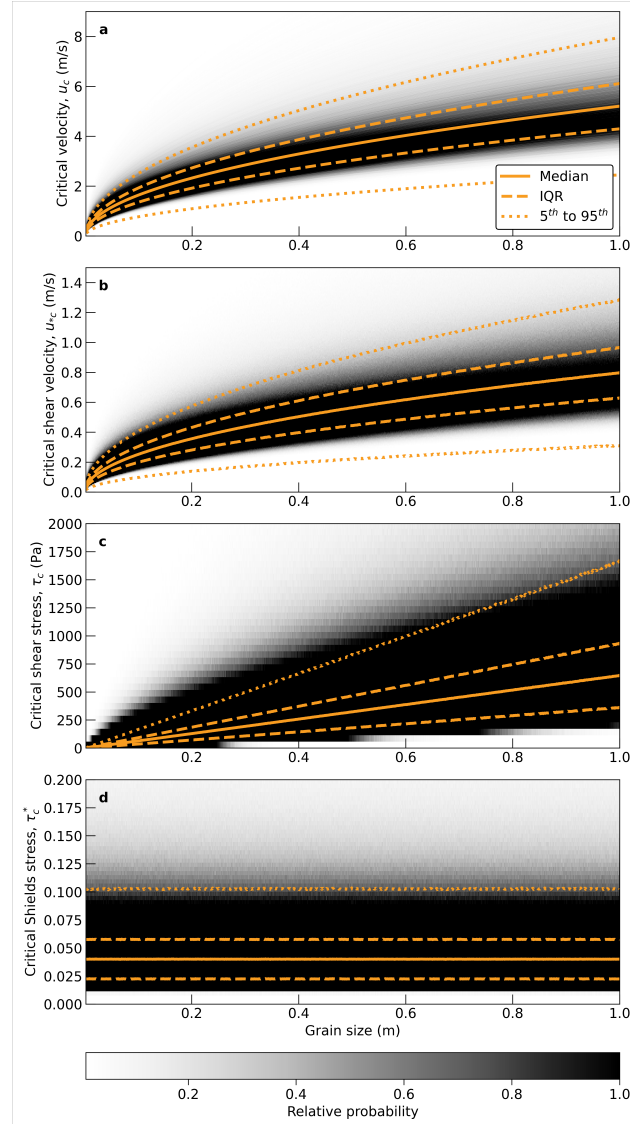


Figure 2. Probability density maps of critical flow properties calculated from force-balance parameter distributions specified in Table 1. Distribution of critical velocity (a), critical shear velocity (b), critical shear stress (c) and critical Shields stress (d) as a function of grain size found using a Monte Carlo Method to propagate variability of the force-balance parameters through a grain-scale force balance. Solid lines show power law fits to median values, long-dashed lines show the interquartile range and dotted lines show power law fit to the 5th to 95th percentile values. Black to gray shading shows density of values from the Monte Carlo method divided by the maximum density and is defined as the ‘relative probability’ in the colorbar.

495 an effective coefficient of friction to reflect geometric resistance to motion for a grain
 496 that will be mobilized via rolling, resulting in an inherently lower effective frictional
 497 resistance. For Wu and Shih (2012) Experiment 1, in which the mobilizing particle
 498 rotated through the saddle between two downstream particles, we set the mean of the
 499 ϕ distribution to 19 degrees with a range of 9 - 29 degrees to account for potential
 500 asphericity of particles and mobilization not directly through the saddle. In Wu and
 501 Shih (2012) Experiment 2, the grain was forced to exit over or oblique to a downstream
 502 particle and we used a mean μ of 35 degrees and a ϕ range of 25 - 45 degrees. We
 503 assumed a constant $p_* = 0.86$ for both experiments based on the position of the
 504 mobilized particle prior to entrainment. We held ρ and ρ_s constant to reflect the
 505 values from the study. Lacking additional constraints on C_L , we assumed a mean C_L
 506 = 0.19 (half the value of our general case) due to the low flow velocity, and the full
 507 C_L parameter distribution range from the most general case ($0.06 < C_L < 2$) (Table
 508 1). Inputting these experiment-specific distributions into our Monte Carlo simulations
 509 resulted in a best fit $m_c = 2.54 \pm 0.29$ (median +/- interquartile range) for Experiment
 510 1 (Figure 3a) and $m_c = 1.09 \pm 0.18$ for Experiment 2 (Figure 3b).

511 We found that the predicted critical velocity distributions using the simplified
 512 power law (Equation 17) and the updated m_c values (2.54 ± 0.29 for Experiment 1 and
 513 1.09 ± 0.1 for Experiment 2) bound the range of velocities measured immediately before
 514 entrainment across all replicates (Figure 3a-b). Model-predicted critical velocities, in
 515 terms of both the mean and interquartile range, change in concert with the exper-
 516 imental configuration, owing to our use of experimental constraints on C_d , p , ρ , ρ_s , and
 517 ϕ . We interpret this agreement between our theoretical predictions and experimen-
 518 tal observations as evidence that incorporating independently quantified variability
 519 in force-balance parameters allows accurate representation of the distribution of crit-
 520 ical velocities at initiation of sediment motion. This supports our hypothesis that
 521 the variability observed in incipient motion data is encompassed within the expected
 522 variability associated with applicable FBP variability.

523 5.2 Comparison with field data

524 The comparison above represents idealized conditions where many replicates were
 525 used to quantify variability in the threshold velocity; however, such data are rarely
 526 available. We assessed the performance of the simplified family of power laws in less
 527 idealized conditions by comparing model predictions to field and flume data spanning
 528 a variety of incipient motion observation techniques, inferred flow conditions, bed
 529 packing and grain size.

530 5.2.1 Comparison with field measurements of paired incipient motion 531 and grain-scale critical velocity

532 Helley (1969) conducted a unique field experiment placing natural grains (up
 533 to 0.52 m in diameter) on a natural riverbed at low flow and recorded the incipient
 534 motion of these grains with concurrent flow depth. This allowed a threshold grain-
 535 scale flow velocity to be determined using a calibrated stage-velocity relation. To our
 536 knowledge, this is the only incipient motion field data with constraints on grain-scale
 537 flow velocity, and is thus the best suited field data to test our model. We used reported
 538 grain properties (the three primary axes, sediment density and particle volume) and the
 539 inferred relative position within the bed to constrain FBP distributions. Owing to the
 540 nature of grain placement on top of the natural sediment bed, we assumed low frictional
 541 resistance from bed packing and grain burial and therefore used a μ distribution (mean
 542 $\phi = 40^\circ$, standard deviation = 15°) which minimizes the contribution of bed packing
 543 to the effective friction angle (Kirchner et al., 1990). We assumed grains have high
 544 protrusion ($p_* = 0.9 \pm 0.2$). All other FBP distributions followed the distributions

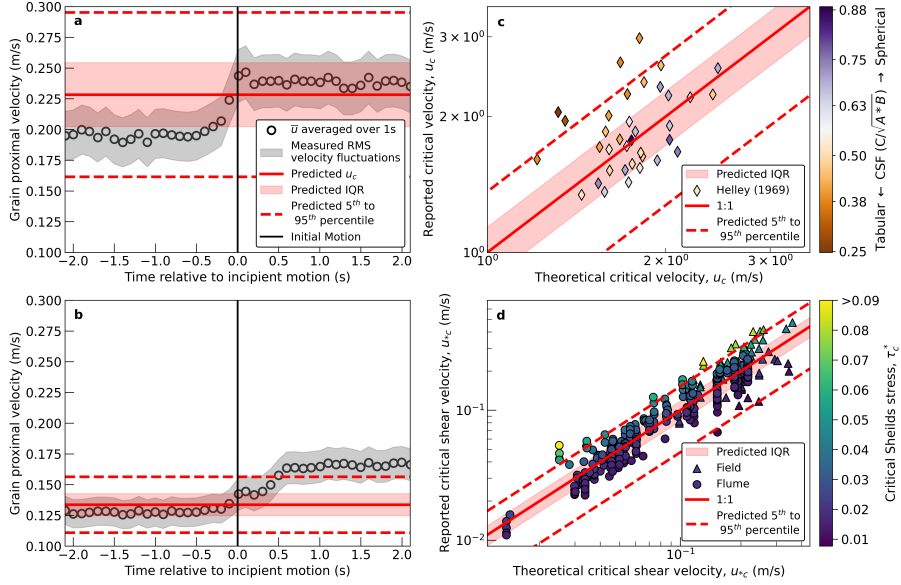


Figure 3. Comparison between model-predicted (red lines and red shading) and experimentally observed (various point symbols) flow conditions at incipient motion. (a and b) Downstream component of the grain-proximal velocity measured using laser Doppler velocimetry by Wu and Shih (2012) in two different bed packing configurations with different grain densities. Open circles indicate mean velocity measurements from all replicate experiments averaged over 0.1 s intervals. Grey shading spans the root-mean-square error of velocity fluctuations measured across all replicate experiments. (c) Observed velocity at incipient motion by Helley (1969) from Blue Creek, CA against expected theoretical critical velocity with points colored by their respective Cory Shape Factor (CSF), where A is the long axis, B is the intermediate axis and C is the short axis. Tabular particles that do not conform to the assumptions used to estimate critical velocity have small CSF , whereas more spherical particles have high CSF . (d) Reported critical shear velocity from compilation of field (triangles) and flume (circles) data against expected theoretical critical shear velocity with point color representing the reported critical Shields stress for data referred to in Section 6.2.2. For all plots, solid lines show the power law for median values, dashed lines show power law for the 5th and 95th percentile values, and colored patches span the interquartile range estimated using the reported grain size.

545 specified in Table 1, these broad values and the physical constraints described above
 546 resulted in a best fit m_c value of 3.77 ± 0.31 .

547 The resulting comparison between modeled and observed critical velocities shows
 548 that the predicted threshold velocity and the interquartile range of uncertainty encom-
 549 pass a majority of the observations for grains that are approximately spherical (Figure
 550 3c). Some of the reported velocities, particularly for tabular grains, are higher than the
 551 interquartile range estimate from our force-balance predictions (Figure 3c), potentially
 552 due to the fact that we use distributions of drag and lift coefficients for approximately
 553 spherical grains, which may systematically overestimate drag and lift coefficients for
 554 tabular grains. We interpret the tight correspondence between observed and predicted
 555 critical velocities and the degree to which a majority of approximately spherical grains
 556 fall within our predicted interquartile range as a second positive test of our hypothesis
 557 that incorporating variability in FBP offers a reasonable estimate of the critical veloc-
 558 ity and variability in that velocity. This second positive test adds additional credibility
 559 to our hypothesis because it was carried out in a natural setting and with significantly
 560 larger grain sizes (up to $D = 0.52$ m) relative to the previous laboratory comparison.

561 ***5.2.2 Comparison with field and flume data of incipient motion with*** 562 ***reach-averaged critical shear velocity***

563 In practice, most field and laboratory data do not allow a direct estimate of
 564 grain-scale flow velocity as in the Wu and Shih (2012) and Helley (1969) datasets. We
 565 tested the ability of our force-balance model to capture variability in incipient motion
 566 using data more commonly collected in the lab and field data. Specifically, we used
 567 a large compilation of estimated critical shear velocity at incipient motion from flume
 568 experiments and field observations (Aguirre-Pe, 1975; Andrews, 1994; Buffington &
 569 Montgomery, 1997; Andrews, 2000; Shvidchenko et al., 2001; Church & Hassan, 2002;
 570 Mueller et al., 2005; Whitaker & Potts, 2007; Scheingross et al., 2013; Prancevic et
 571 al., 2014). Owing to the diversity of field and flume data included in this compilation,
 572 we predicted critical velocities using the most general FBP distributions in Table
 573 1. We assumed a roughness layer height of $k_s = D$ for Equation 14 to maintain
 574 consistency with assumptions in Buffington and Montgomery (1997), this is likely an
 575 underestimate of the true roughness layer height which may result in overestimates of
 576 u_{*c} . We filtered the incipient motion data to include observations with slopes $< 5\%$
 577 and $D_{50} > 0.001$ m, set by the assumptions of our methodology. We observe that
 578 61% of the flume data fall within the interquartile range of our model predictions,
 579 and 95% of flume data fall within the 5 to 95% confidence interval (Figure 3d). Field
 580 data shows a similar consistency with 39% and 90% falling within the IQR and 5 to
 581 95% confidence interval, respectively. We interpret this as additional strong support
 582 of our hypothesis that incorporating known variability in FBP can explain observed
 583 variability in thresholds at incipient motion.

584 While the majority of data fall within our predicted variability bounds, the pre-
 585 dicted critical shear velocity is biased high (i.e., a majority of points plot below the
 586 one-to-one line). One potential explanation for this bias is the assumption of spherical
 587 grains which may overestimate grain volume, thus requiring a higher estimated critical
 588 shear velocity to mobilize the grains than observed. An additional source of variability
 589 not included in our analysis is the variability that might result from mixing measure-
 590 ment techniques and definitions for incipient motion, which in the compilation include
 591 defining a non-zero sediment flux, visual observation of initial to full bed mobility,
 592 empirical competence and theoretical estimates for a given flow condition (Buffington
 593 & Montgomery, 1997). Despite this additional variability, we are able to estimate
 594 the range of threshold conditions observed across decades of incipient motion studies
 595 through incorporating expected variability in the forces controlling entrainment.

5.3 Estimating expected variability in bedload flux

Bedload flux is characterized by large fluctuations, particularly when flow conditions are near the threshold of motion (e.g., Figure 4 and Ancey et al. (2008)). Following from the early work of Einstein (1950), there has been renewed interest in stochastic formulations to predict bedload flux and observed variability (Seminara et al., 2002; Ancey, 2010; Fofoula-Georgiou & Stark, 2010; Turowski, 2010; Furbish et al., 2012; Ancey & Heyman, 2014; Fathel et al., 2015; Heyman et al., 2016; Ancey & Pascal, 2020; Benavides et al., 2022; Pierce et al., 2022). Despite these attempts that offer new theory to estimate and explain observed variability in bedload flux, empirical, deterministic formulations are still the most common approach to quantifying bedload flux (e.g., Meyer-Peter & Müller, 1948; Fernandez Luque & Van Beek, 1976; Wong & Parker, 2006). Here we present a method that incorporates the expected variability in incipient motion developed above, and that includes variability in fluid stress and bed configuration, to offer bounds of expected variability on commonly applied deterministic bedload flux formulations.

The most commonly used formulae to estimate bedload transport take the form of

$$q_* = a(\tau^* - \tau_c^*)^b \quad (22)$$

where $q_* = q_s/(RgD^3)$ is a non-dimensional bedload flux per unit width, q_s is the volumetric bedload flux per unit width, $R = (\rho_s - \rho)/\rho$ and a and b are empirically-derived constants (e.g., Meyer-Peter & Müller, 1948; Fernandez Luque & Van Beek, 1976; Wong & Parker, 2006). Inspection of Equation 22 highlights that small variation in τ_c^* can lead to large variations in bedload flux estimates, due to the non-linear dependence of sediment flux on excess Shield stress ($\tau^* - \tau_c^*$).

To illustrate how variability in the threshold of motion can be propagated to estimate expected variability in sediment flux, we used our framework to add variability to the well-established Wong and Parker (2006) bedload flux empirical relationship,

$$q_* = 4.93(\tau^* - \tau_c^*)^{1.60} \quad (23)$$

where Wong and Parker (2006) set $\tau_c^* = 0.0470$ based on a best fit to data. We use our Monte Carlo method to assess variability around $\tau_c^* = 0.0470$. To reproduce this τ_c^* value, we assume all FBPs follow the most general distributions from Table 1, but we set mean $p_* = 0.3$ to increase τ_c^* from our estimate of 0.040 to the 0.047 best fit from (Wong & Parker, 2006). This results in an interquartile range of τ_c^* values ranging from $0.025 < \tau_c^* < 0.69$, or $\tau_c^* = 0.047 \pm 0.022$.

The expected variability around the Wong and Parker (2006) relationship derived from our force-balance framework accounts for 89% of the observed variability in the bedload flux measurements on which the Wong and Parker relationship was originally calibrated Figure 4. One potential reason our variability estimates encompass 89% of the data, even though it is based on the interquartile range of expected τ_c^* values, is because we used the full range of FBP distributions in Table 1. This variability could be reduced if FBP measurements were available for the sediment flux data, in which case we would expect the predicted variability to encompass closer to 50% of the data. Regardless, we interpret the fact that variability from our framework encompasses the observed data to suggest that variability in incipient motion from force-balance parameters can be used to better constrain expected variation in sediment flux.

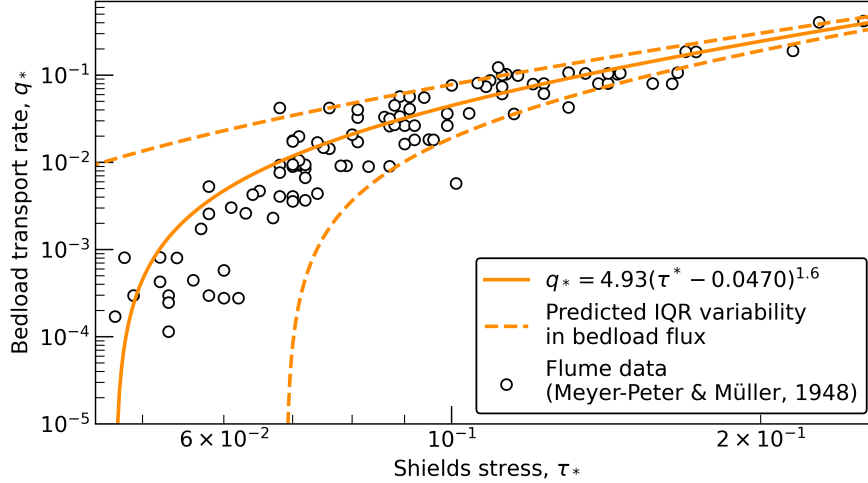


Figure 4. Comparison of flume-measured bedload flux (Meyer-Peter & Müller, 1948) with the Wong and Parker (2006) empirical fit. Interquartile range of variability on τ_c^* predicted using the framework developed here (see text for details). q_* is the dimensionless volume bedload flux per unit width and τ^* is the Shields stress.

639

6 Discussion

640

641

642

643

644

645

646

Our results demonstrate that the magnitude of scatter observed in flow metrics at that time of incipient motion is predictable and is encompassed within the variability expected from independently quantified and site-specific distributions of force-balance parameters (Figure 3). Furthermore, our results provide a simple method to constrain expected variability in the threshold of motion using a power law function, $u_c = m_c D^{0.5}$, where the power law coefficient, m_c , changes to encompass expected FBP variability.

647

648

649

650

651

652

653

654

655

656

657

658

659

660

The power law relationship between critical velocity and sediment size has been observed empirically for centuries (Brahm, 1753; Leliavsky, 1955; Strand, 1973) and is a natural result when formulating a grain-scale force balance to solve for a critical velocity (Wiberg & Smith, 1987, Equation 10). The novel result found here is that the degree of variation on the power law coefficient is predictable based on independent laboratory and field measurements of parameters used to close the force balance (Figure 3), and that this variability is most often dominated by variability in the distributions of effective lift, drag and protrusion (Figure 1d). When the expected variability in force-balance parameters is explicitly incorporated, the resulting threshold of motion distributions show that substantial deviations from commonly assumed values (e.g., $\tau_c^* = 0.045$) are possible (Figure 2). The modeling framework presented here allows the observed FBP variability to be easily propagated to estimated the expected variability of critical velocity, critical shear stress or critical Shields stress allowing for more robust, even if uncertain, estimates of incipient-motion thresholds.

661

662

663

664

665

666

667

While our analysis used a Monte Carlo method to propagate FBP variability to variability in incipient motion, we show that the threshold of motion can be described by a family of easy-to-use power laws describing both the mean and variability about the mean for incipient motion as a function of grain size. To aid in rapid calculation of expected variability in incipient motion thresholds we compiled a table of power law fit coefficients (m , i.e., m_c , m_* , m_τ , and τ_c^*) with associated variability that span flow, grain and bed conditions that are likely to be encountered on Earth and other

668 planetary bodies (Table S1). If little information is known about the site and flows
 669 expected there, the most variable m values presented in Section 4 should provide
 670 robust estimates that incorporate the possibility of broad variability due to the lack
 671 of site-specific values for FBPs. If it is possible to inform the expected distribution of
 672 flow velocities, bed conditions, grain or fluid properties, then one can better constrain
 673 the variability in the m value selected and reduce the expected variability in incipient
 674 motion.

675 To facilitate easy selection of m for the most readily constrained bed properties
 676 of ϕ and p_* we compiled m values and variability by varying mean values of ϕ and
 677 p_* (Figure 5). These results highlight how the expected m_c , m_* , m_τ , and τ_c^* and
 678 associated variability change when shifting the mean of two FBPs from those presented
 679 in Table 1. These plots also highlight that changing mean parameter values, such as
 680 the effective friction coefficient $\mu = \tan(\phi)$, can have a large impact on the expected
 681 critical velocity (as seen by the notable increases in m as a function of ϕ in Figure 5).
 682 This is despite μ being one of the smaller contributors to the expected variance in u_c
 683 distributions (Figure 1d) owing to the relatively small variance relative to the mean
 684 found in many field-measured ϕ distributions (e.g., Hodge et al., 2013; Prancevic &
 685 Lamb, 2015). This variability in the respective m values also informs our intuition of
 686 how small changes in bed configuration, expressed through ϕ and p_* , may influence
 687 incipient-motion thresholds and how these parameters may change as a fluvial system
 688 evolves (Masteller et al., 2019).

689 Our results highlight that expected variability in incipient sediment motion can
 690 be related to FBP variability. As more FBP distributions become available, we will
 691 be able to decrease the variability in our predictions of the onset of incipient motion
 692 for particular flow and bed conditions. The results from our global sensitivity analy-
 693 sis highlight that variability in the distributions of effective lift, drag and protrusion
 694 are the current largest contributors to variability in critical velocity (Figure 1), and
 695 hence are obvious targets for further study. However, further investigation into FBP
 696 distributions might reveal that substantial variation in some FBPs is to be expected in
 697 certain flow and bed conditions such that there will be fundamental limits as to how
 698 small variability in critical velocity thresholds could become. For example, if future
 699 investigations continue to show broad distributions in C_D , the distributions of critical
 700 velocity cannot become tighter than the variance contributed by the C_D distribution.

701 While the framework presented here represents a simple and straightforward way
 702 to account for variability in incipient motion, additional improvement could be made
 703 by substituting our descriptions of drag, lift, and frictional forces for expressions that
 704 explicitly account for different mechanisms promoting or resisting grain entrainment,
 705 as opposed to lumping the effects of multiple mechanisms into simplified expressions
 706 with effective coefficients. The simplified expressions used here rely on effective param-
 707 eters, making it difficult to directly attribute threshold variability to measurable flow,
 708 grain or bed properties. For example, Schmeeckle et al. (2007) presents a derivation
 709 of the nominal drag force acting on a stationary particle that could be implemented
 710 in our framework to more closely scrutinize the effect of 3D grain-fluid interactions for
 711 grain entrainment in laminar, transitional, or turbulent flow. The lift force, however,
 712 is a more complicated component to implement as there is a lack of general agreement
 713 on how to properly quantify or estimate the influence of lift on grain entrainment (as
 714 discussed in Dey et al. (2020)); further work is required to refine the quantitative de-
 715 scription of lift before incorporation into the framework presented here. Recent work
 716 from Yager, Schmeeckle, and Badoux (2018) proposes three separate equations, each
 717 with unique measurable bed and grain parameters to explicitly describe resisting forces
 718 resulting from pocket geometry, grain burial, and bed packing. Incorporating these
 719 equations, as opposed to lumping all effects into a single simplified effective friction
 720 rule (as we have done), would be a clear improvement once sufficient measurements

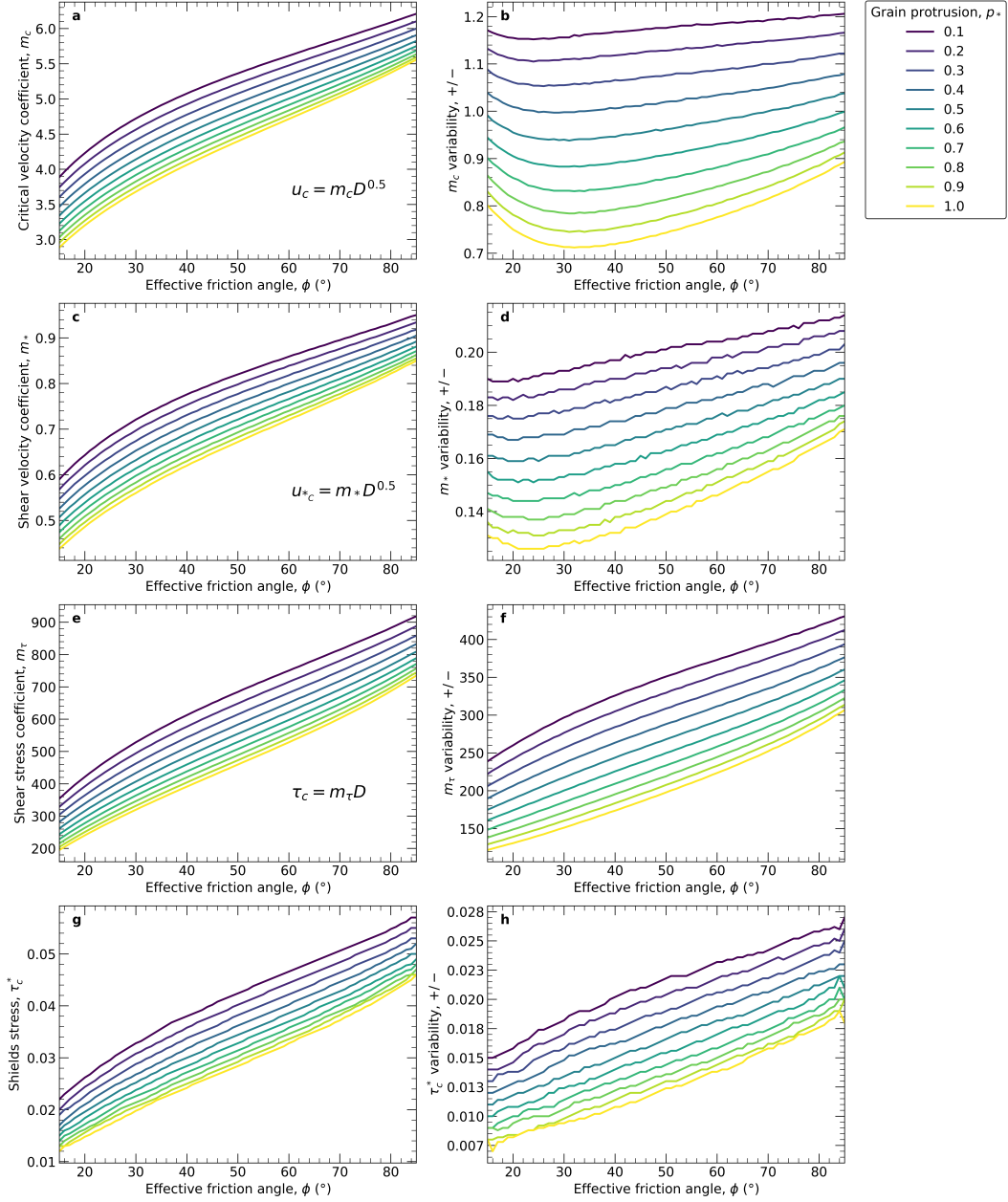


Figure 5. Best-fit power law coefficients (i.e., m_c , m_* , m_τ , and τ_c^*) as a result of altering the assumed mean of the effective friction angle (ϕ) and the relative grain protrusion (p_*). Best-fit power law coefficients and associated variability (IQR, +/-) for (a and b) critical velocity (u_c), (c and d) critical shear velocity (u_{*c}), and (e and f) critical shear stress (τ_c). (g and h) critical Shields stress (τ_c^*) and associated variability. m_c , m_* , m_τ and τ_c^* displayed as a function of mean ϕ and colored by mean p_* . All other force-balance parameter distributions are as specified in Table 1.

721 have been made. Even though our investigation into potential impacts of covariability
 722 between parameters revealed only second-order importance (Figure S1), explicitly ac-
 723 counting for co-variability in FBPs such as is probable between C_D and C_L for a given
 724 bed packing or grain protrusion scenario may lead to more accurate representations
 725 of threshold distributions (Schmeeckle et al., 2007; Dwivedi et al., 2011). As addi-
 726 tional field and laboratory measurements become available, substituting these refined
 727 parameter distributions into the current framework should increase the robustness of
 728 output threshold distributions as well as increase the ability to select more accurate
 729 FBP distributions based on independent field and laboratory measurements.

730 7 Conclusions

731 Our results demonstrate that the magnitude of scatter observed in incipient mo-
 732 tion is predictable and is encompassed within the variability expected from indepen-
 733 dently quantified and site-specific variability in the force-balance parameters. This
 734 threshold of motion can be described by a family of easy-to-use power laws describing
 735 both the mean and variability about the mean for incipient motion as a function of
 736 grain size. The degree of variation on the power law coefficient is predictable based
 737 on independent measurements of force-balance parameters and that this variability is
 738 most often dominated by variability in the distributions of effective lift, drag and pro-
 739 trusion. As more force-balance parameter distributions become available, we will be
 740 able to make more accurate estimates of expected variability at the onset of incipient
 741 motion for particular flow and bed conditions. When such constraints are lacking,
 742 using broadly applicable force-balance distributions accurately characterizes variabil-
 743 ity observed across diverse field settings. Thus, while variability in incipient sediment
 744 motion will always persist, having a means of assessing that variability should allow
 745 for more robust estimates of sediment transport across environmental conditions and
 746 planetary bodies.

747 Acknowledgements

748 We thank Jeff Prancevic for sharing compiled incipient motion data, Fu-Chun
 749 Wu and Wu-Rong Shih for sharing incipient motion flume data, Elowyn Yager for
 750 sharing in-situ observations of relative protrusion, and Editor Ton Hoitink, Asso-
 751 ciate Editor Christophe Ancey and three anonymous reviewers for comments that
 752 improved the quality of this manuscript. This work was supported by NASA awards
 753 80NSSC19K0165 and 80NSSC20K1343 to SWM.

754 Open Research

755 The data and codes associated with this manuscript are available through Figshare:
 756 <https://doi.org/10.6084/m9.figshare.22266187> (Feehan et al., 2023). We used
 757 version 6.14 of Dakota for the sensitivity analysis. The application was built from
 758 source code available from the Dakota Git repository available at [https://dakota](https://dakota.sandia.gov/)
 759 [.sandia.gov/](https://dakota.sandia.gov/) using repository revision 382229e53 (McKenna et al., 2021).

760 References

- 761 Aguirre-Pe, J. (1975). Incipient erosion in high gradient open channel flow with
 762 artificial roughness elements. *Proc. 16th Congr. Int. Assoc. Hydraul. Res. San*
 763 *Paulo Brazil*(2), 137–180. (Aguirre-Pe, J. (1975). Incipient erosion in high gra-
 764 dient open channel flow with artificial roughness elements. Proc. 16th Congr.
 765 Int. Assoc. Hydraul. Res. San Paulo Brazil, 2, 137-180.)
 766 Ali, S. Z., & Dey, S. (2016, July). Hydrodynamics of sediment threshold. *Physics*

- 767 *of Fluids*, 28(7), 075103. Retrieved 2023-02-01, from [http://aip.scitation](http://aip.scitation.org/doi/10.1063/1.4955103)
768 [.org/doi/10.1063/1.4955103](http://aip.scitation.org/doi/10.1063/1.4955103) doi: 10.1063/1.4955103
- 769 Ali, S. Z., & Dey, S. (2018, April). Impact of phenomenological theory of tur-
770 bulence on pragmatic approach to fluvial hydraulics. *Physics of Fluids*,
771 30(4), 045105. Retrieved 2023-02-03, from [http://aip.scitation.org/](http://aip.scitation.org/doi/10.1063/1.5025218)
772 [doi/10.1063/1.5025218](http://aip.scitation.org/doi/10.1063/1.5025218) doi: 10.1063/1.5025218
- 773 Ancey, C. (2010, June). Stochastic modeling in sediment dynamics: Exner equa-
774 tion for planar bed incipient bed load transport conditions: STOCHASTIC
775 MODELING IN SEDIMENT DYNAMICS. *Journal of Geophysical Research:*
776 *Earth Surface*, 115(F2). Retrieved 2023-07-29, from [http://doi.wiley.com/](http://doi.wiley.com/10.1029/2009JF001260)
777 [10.1029/2009JF001260](http://doi.wiley.com/10.1029/2009JF001260) doi: 10.1029/2009JF001260
- 778 Ancey, C., Davison, A. C., Böhm, T., Jodeau, M., & Frey, P. (2008, Jan-
779 uary). Entrainment and motion of coarse particles in a shallow wa-
780 ter stream down a steep slope. *Journal of Fluid Mechanics*, 595, 83–
781 114. Retrieved 2023-07-29, from [https://www.cambridge.org/core/](https://www.cambridge.org/core/product/identifier/S0022112007008774/type/journal_article)
782 [product/identifier/S0022112007008774/type/journal_article](https://www.cambridge.org/core/product/identifier/S0022112007008774/type/journal_article) doi:
783 10.1017/S0022112007008774
- 784 Ancey, C., & Heyman, J. (2014, April). A microstructural approach to bed load
785 transport: mean behaviour and fluctuations of particle transport rates. *Jour-*
786 *nal of Fluid Mechanics*, 744, 129–168. Retrieved 2023-07-29, from [https://](https://www.cambridge.org/core/product/identifier/S0022112014000743/type/journal_article)
787 [www.cambridge.org/core/product/identifier/S0022112014000743/type/](https://www.cambridge.org/core/product/identifier/S0022112014000743/type/journal_article)
788 [journal_article](https://www.cambridge.org/core/product/identifier/S0022112014000743/type/journal_article) doi: 10.1017/jfm.2014.74
- 789 Ancey, C., & Pascal, I. (2020, July). Estimating Mean Bedload Transport Rates
790 and Their Uncertainty. *Journal of Geophysical Research: Earth Surface*,
791 125(7). Retrieved 2023-07-21, from [https://onlinelibrary.wiley.com/doi/](https://onlinelibrary.wiley.com/doi/10.1029/2020JF005534)
792 [10.1029/2020JF005534](https://onlinelibrary.wiley.com/doi/10.1029/2020JF005534) doi: 10.1029/2020JF005534
- 793 Andrews, E. D. (1994, July). Marginal bed load transport in a gravel bed stream,
794 Sagehen Creek, California. *Water Resources Research*, 30(7), 2241–2250. Re-
795 trieved 2022-02-20, from <http://doi.wiley.com/10.1029/94WR00553> doi: 10
796 .1029/94WR00553
- 797 Andrews, E. D. (2000, February). Bed material transport in the Virgin River,
798 Utah. *Water Resources Research*, 36(2), 585–596. Retrieved 2022-02-
799 20, from <http://doi.wiley.com/10.1029/1999WR900257> doi: 10.1029/
800 1999WR900257
- 801 Baker, V. R. (2002, March). The study of superfoods. *Science*, 295(5564), 2379–
802 2380. Retrieved 2021-11-12, from [https://www.science.org/doi/10.1126/](https://www.science.org/doi/10.1126/science.1068448)
803 [science.1068448](https://www.science.org/doi/10.1126/science.1068448) doi: 10.1126/science.1068448
- 804 Benavides, S. J., Deal, E., Rushlow, M., Venditti, J. G., Zhang, Q., Kamrin, K., &
805 Perron, J. T. (2022, March). The Impact of Intermittency on Bed Load Sed-
806 iment Transport. *Geophysical Research Letters*, 49(5). Retrieved 2023-07-21,
807 from <https://onlinelibrary.wiley.com/doi/10.1029/2021GL096088> doi:
808 10.1029/2021GL096088
- 809 Booth, A. M., Hurley, R., Lamb, M. P., & Andrade, J. E. (2014, December). Force
810 chains as the link between particle and bulk friction angles in granular mate-
811 rial: Granular force chains and friction angle. *Geophysical Research Letters*,
812 41(24), 8862–8869. Retrieved 2021-11-12, from [http://doi.wiley.com/](http://doi.wiley.com/10.1002/2014GL061981)
813 [10.1002/2014GL061981](http://doi.wiley.com/10.1002/2014GL061981) doi: 10.1002/2014GL061981
- 814 Brahms, A. (1753). Anfangsgrunde der deich und wasserbaukunst Aurich.
- 815 Bridge, J. S., & Bennett, S. J. (1992, February). A model for the entrainment
816 and transport of sediment grains of mixed sizes, shapes, and densities.
817 *Water Resources Research*, 28(2), 337–363. Retrieved 2023-03-03, from
818 <http://doi.wiley.com/10.1029/91WR02570> doi: 10.1029/91WR02570
- 819 Buffington, J. M., & Montgomery, D. R. (1997, August). A systematic analy-
820 sis of eight decades of incipient motion studies, with special reference to
821 gravel-bedded rivers. *Water Resources Research*, 33(8), 1993–2029. Re-

- 822 trieved 2021-11-12, from <http://doi.wiley.com/10.1029/96WR03190> doi:
823 10.1029/96WR03190
- 824 Celik, A. O., Diplas, P., & Dancy, C. L. (2013, April). Instantaneous turbulent
825 forces and impulse on a rough bed: Implications for initiation of bed mate-
826 rial movement: Instantaneous turbulent forces and impulse on a rough bed.
827 *Water Resources Research*, *49*(4), 2213–2227. Retrieved 2022-04-06, from
828 <http://doi.wiley.com/10.1002/wrcr.20210> doi: 10.1002/wrcr.20210
- 829 Chiew, Y. M., & Parker, G. (1995). Reply to discussion of: Incipient sediment mo-
830 tion on non-horizontal slopes. *J. of Hydraulic Research, IAHR*(33(5)), 729–
831 730.
- 832 Christensen, B. A. (1995, September). Incipient Sediment Motion On Non-
833 Horizontal Slopes. *Journal of Hydraulic Research*, *33*(5), 725–730. Retrieved
834 from <https://doi.org/10.1080/00221689509498569> (Publisher: Taylor &
835 Francis) doi: 10.1080/00221689509498569
- 836 Church, M., & Hassan, M. A. (2002, November). Mobility of bed material in Har-
837 ris Creek. *Water Resources Research*, *38*(11), 19–1–19–12. Retrieved 2022-
838 02-20, from <http://doi.wiley.com/10.1029/2001WR000753> doi: 10.1029/
839 2001WR000753
- 840 Church, M., Hassan, M. A., & Wolcott, J. F. (1998, November). Stabilizing
841 self-organized structures in gravel-bed stream channels: Field and experi-
842 mental observations. *Water Resources Research*, *34*(11), 3169–3179. Re-
843 trieved 2021-11-12, from <http://doi.wiley.com/10.1029/98WR00484> doi:
844 10.1029/98WR00484
- 845 Deal, E., Venditti, J. G., Benavides, S. J., Bradley, R., Zhang, Q., Kamrin, K.,
846 & Perron, J. T. (2023, January). Grain shape effects in bed load sedi-
847 ment transport. *Nature*, *613*(7943), 298–302. Retrieved 2023-02-01,
848 from <https://www.nature.com/articles/s41586-022-05564-6> doi:
849 10.1038/s41586-022-05564-6
- 850 Dey, S., & Ali, S. Z. (2017a, November). Mechanics of Sediment Transport: Partic-
851 le Scale of Entrainment to Continuum Scale of Bedload Flux. *Journal of En-*
852 *gineering Mechanics*, *143*(11), 04017127. Retrieved 2023-02-03, from [https://](https://ascelibrary.org/doi/10.1061/%28ASCE%29EM.1943-7889.0001343)
853 ascelibrary.org/doi/10.1061/%28ASCE%29EM.1943-7889.0001343 doi: 10
854 .1061/(ASCE)EM.1943-7889.0001343
- 855 Dey, S., & Ali, S. Z. (2017b, May). Stochastic mechanics of loose boundary parti-
856 cle transport in turbulent flow. *Physics of Fluids*, *29*(5), 055103. Retrieved
857 2023-02-03, from <http://aip.scitation.org/doi/10.1063/1.4984042> doi:
858 10.1063/1.4984042
- 859 Dey, S., & Ali, S. Z. (2018, June). Review Article: Advances in modeling of bed
860 particle entrainment sheared by turbulent flow. *Physics of Fluids*, *30*(6),
861 061301. Retrieved 2023-02-03, from [http://aip.scitation.org/doi/](http://aip.scitation.org/doi/10.1063/1.5030458)
862 [10.1063/1.5030458](http://aip.scitation.org/doi/10.1063/1.5030458) doi: 10.1063/1.5030458
- 863 Dey, S., Ali, S. Z., & Padhi, E. (2020, June). Hydrodynamic Lift on Sedi-
864 ment Particles at Entrainment: Present Status and Its Prospect. *Journal*
865 *of Hydraulic Engineering*, *146*(6), 03120001. Retrieved 2023-04-15, from
866 <https://ascelibrary.org/doi/10.1061/%28ASCE%29HY.1943-7900.0001751>
867 doi: 10.1061/(ASCE)HY.1943-7900.0001751
- 868 Diplas, P., Dancy, C. L., Celik, A. O., Valyrakis, M., Greer, K., & Akar, T. (2008,
869 October). The Role of Impulse on the Initiation of Particle Movement Under
870 Turbulent Flow Conditions. *Science*, *322*(5902), 717–720. Retrieved 2021-11-
871 12, from <https://www.science.org/doi/10.1126/science.1158954> doi: 10
872 .1126/science.1158954
- 873 Dwivedi, A., Melville, B. W., Shamseldin, A. Y., & Guha, T. K. (2011, June). Anal-
874 ysis of hydrodynamic lift on a bed sediment particle: ANALYSIS OF LIFT
875 ON A SEDIMENT PARTICLE. *Journal of Geophysical Research: Earth Sur-*
876 *face*, *116*(F2). Retrieved 2023-02-03, from <http://doi.wiley.com/10.1029/>

- 877 2009JF001584 doi: 10.1029/2009JF001584
- 878 Einstein, H. A. (1950). The Bed-Load Function for Sediment Transportation in
879 Open Channel Flows. *United States Department of Agriculture, No. 1026*.
- 880 Einstein, H. A., & El-Samni, E.-S. A. (1949, July). Hydrodynamic Forces on a
881 Rough Wall. *Reviews of Modern Physics*, 21(3), 520–524. Retrieved 2021-11-
882 12, from <https://link.aps.org/doi/10.1103/RevModPhys.21.520> doi: 10.
883 .1103/RevModPhys.21.520
- 884 Fathel, S. L., Furbish, D. J., & Schmeeckle, M. W. (2015, November). Experimental
885 evidence of statistical ensemble behavior in bed load sediment transport.
886 *Journal of Geophysical Research: Earth Surface*, 120(11), 2298–2317. Re-
887 trieved 2023-07-29, from [https://onlinelibrary.wiley.com/doi/10.1002/
888 2015JF003552](https://onlinelibrary.wiley.com/doi/10.1002/2015JF003552) doi: 10.1002/2015JF003552
- 889 Feehan, S. A., McCoy, S. W., Scheingross, J. S., & Gardner, M. H. (2023). *Quantify-*
890 *ing variability of incipient-motion thresholds in gravel-bedded rivers using a*
891 *grain-scale force-balance model: Software and Dataset*. figshare. Retrieved from
892 <https://doi.org/10.6084/m9.figshare.22266187>
- 893 Ferguson, R., & Church, M. (2004, November). A Simple Universal Equation for
894 Grain Settling Velocity. *Journal of Sedimentary Research*, 74(6), 933–937.
895 Retrieved 2021-11-12, from [https://pubs.geoscienceworld.org/jsedres/
896 article/74/6/933-937/99413](https://pubs.geoscienceworld.org/jsedres/article/74/6/933-937/99413) doi: 10.1306/051204740933
- 897 Fernandez Luque, R., & Van Beek, R. (1976, April). Erosion And Transport Of
898 Bed-Load Sediment. *Journal of Hydraulic Research*, 14(2), 127–144. Re-
899 trieved 2021-11-12, from [http://www.tandfonline.com/doi/abs/10.1080/
900 00221687609499677](http://www.tandfonline.com/doi/abs/10.1080/00221687609499677) doi: 10.1080/00221687609499677
- 901 Fofoula-Georgiou, E., & Stark, C. (2010, June). Introduction to special section on
902 Stochastic Transport and Emergent Scaling on Earth’s Surface: Rethinking ge-
903 omorphic transport-Stochastic theories, broad scales of motion and nonlocality:
904 INTRODUCTION. *Journal of Geophysical Research: Earth Surface*, 115(F2).
905 Retrieved 2023-07-29, from <http://doi.wiley.com/10.1029/2010JF001661>
906 doi: 10.1029/2010JF001661
- 907 Furbish, D. J., Haff, P. K., Roseberry, J. C., & Schmeeckle, M. W. (2012, Septem-
908 ber). A probabilistic description of the bed load sediment flux: 1. Theory:
909 BED LOAD FLUX, 1. *Journal of Geophysical Research: Earth Surface*,
910 117(F3), n/a–n/a. Retrieved 2023-07-21, from [http://doi.wiley.com/
911 10.1029/2012JF002352](http://doi.wiley.com/10.1029/2012JF002352) doi: 10.1029/2012JF002352
- 912 Garcia, M. (Ed.). (2008). *Sedimentation Engineering: Processes, Measurements,*
913 *Modeling, and Practice*. Reston, VA: American Society of Civil Engineers.
914 Retrieved 2023-02-19, from [http://ascelibrary.org/doi/book/10.1061/
915 9780784408148](http://ascelibrary.org/doi/book/10.1061/9780784408148) doi: 10.1061/9780784408148
- 916 Gessler, J. (1971). Beginning and ceasing of sediment motion. *River mechanics*,
917 1(1)(7-1). (Gessler, J. (1971). Beginning and ceasing of sediment motion. River
918 mechanics, 1(1), 7-1.)
- 919 Grant, G. E. (1997, February). Critical flow constrains flow hydraulics in mobile-bed
920 streams: A new hypothesis. *Water Resources Research*, 33(2), 349–358. Re-
921 trieved 2022-04-13, from <http://doi.wiley.com/10.1029/96WR03134> doi: 10.
922 .1029/96WR03134
- 923 Grass, A. J. (1970, March). Initial Instability of Fine Bed Sand. *Jour-*
924 *nal of the Hydraulics Division*, 96(3), 619–632. Retrieved 2021-11-12,
925 from <http://ascelibrary.org/doi/10.1061/JYCEAJ.0002369> doi:
926 10.1061/JYCEAJ.0002369
- 927 Hassan, M. A., Saletti, M., Johnson, J. P. L., Ferrer-Boix, C., Venditti, J. G., &
928 Church, M. (2020, December). Experimental Insights Into the Threshold of
929 Motion in Alluvial Channels: Sediment Supply and Streambed State. *Jour-*
930 *nal of Geophysical Research: Earth Surface*, 125(12). Retrieved 2021-11-12,
931 from <https://onlinelibrary.wiley.com/doi/10.1029/2020JF005736> doi:

- 10.1029/2020JF005736
- 932 Helley, E. J. (1969). Field measurement of the initiation of large bed particle motion
933 in Blue Creek near Klamath, California. *US Government Printing Office*.
- 934 Heyman, J., Bohorquez, P., & Ancey, C. (2016, October). Entrainment, motion,
935 and deposition of coarse particles transported by water over a sloping mo-
936 bile bed: TRANSPORT OF COARSE PARTICLES IN WATER. *Journal*
937 *of Geophysical Research: Earth Surface*, 121(10), 1931–1952. Retrieved
938 2023-07-29, from <http://doi.wiley.com/10.1002/2015JF003672> doi:
939 10.1002/2015JF003672
- 940 Hodge, R. A., Sear, D. A., & Leyland, J. (2013, April). Spatial variations
941 in surface sediment structure in riffle-pool sequences: a preliminary test
942 of the Differential Sediment Entrainment Hypothesis (DSEH): Spatial
943 Variations in Sediment Structure in Riffle-Pool Sequences. *Earth Sur-*
944 *face Processes and Landforms*, 38(5), 449–465. Retrieved 2021-11-12,
945 from <https://onlinelibrary.wiley.com/doi/10.1002/esp.3290> doi:
946 10.1002/esp.3290
- 947 Hurst, A. A., Anderson, R. S., & Crimaldi, J. P. (2021, May). Toward Entrain-
948 ment Thresholds in Fluvial Plucking. *Journal of Geophysical Research: Earth*
949 *Surface*, 126(5). Retrieved 2021-11-12, from [https://onlinelibrary.wiley](https://onlinelibrary.wiley.com/doi/10.1029/2020JF005944)
950 [.com/doi/10.1029/2020JF005944](https://onlinelibrary.wiley.com/doi/10.1029/2020JF005944) doi: 10.1029/2020JF005944
- 951 James, C. S. (1990, January). Prediction of entrainment conditions for nonuniform,
952 noncohesive sediments. *Journal of Hydraulic Research*, 28(1), 25–41. Re-
953 trieved 2021-11-12, from [https://www.tandfonline.com/doi/full/10.1080/](https://www.tandfonline.com/doi/full/10.1080/00221689009499145)
954 [00221689009499145](https://www.tandfonline.com/doi/full/10.1080/00221689009499145) doi: 10.1080/00221689009499145
- 955 Johnston, C. E., Andrews, E. D., & Pitlick, J. (1998, August). In situ determination
956 of particle friction angles of fluvial gravels. *Water Resources Research*, 34(8),
957 2017–2030. Retrieved 2021-11-21, from [http://doi.wiley.com/10.1029/](http://doi.wiley.com/10.1029/98WR00312)
958 [98WR00312](http://doi.wiley.com/10.1029/98WR00312) doi: 10.1029/98WR00312
- 959 Kirchner, J. W., Dietrich, W. E., Iseya, F., & Ikeda, H. (1990, August). The
960 variability of critical shear stress, friction angle, and grain protrusion in
961 water-worked sediments. *Sedimentology*, 37(4), 647–672. Retrieved
962 2022-04-06, from [https://onlinelibrary.wiley.com/doi/10.1111/](https://onlinelibrary.wiley.com/doi/10.1111/j.1365-3091.1990.tb00627.x)
963 [j.1365-3091.1990.tb00627.x](https://onlinelibrary.wiley.com/doi/10.1111/j.1365-3091.1990.tb00627.x) doi: 10.1111/j.1365-3091.1990.tb00627.x
- 964 Komar, P. D., & Clemens, K. E. (1986). The Relationship Between a Grain's
965 Settling Velocity and Threshold of Motion Under Unidirectional Currents.
966 *SEPM Journal of Sedimentary Research*, Vol. 56. Retrieved 2021-11-12, from
967 [https://pubs.geoscienceworld.org/jsedres/article/56/2/258-266/](https://pubs.geoscienceworld.org/jsedres/article/56/2/258-266/113721)
968 [113721](https://pubs.geoscienceworld.org/jsedres/article/56/2/258-266/113721) doi: 10.1306/212F88DC-2B24-11D7-8648000102C1865D
- 969 Lamb, M. P., Brun, F., & Fuller, B. M. (2017a, September). Direct measurements
970 of lift and drag on shallowly submerged cobbles in steep streams: Implications
971 for flow resistance and sediment transport. *Water Resources Research*, 53(9),
972 7607–7629. Retrieved 2021-11-12, from [https://onlinelibrary.wiley.com/](https://onlinelibrary.wiley.com/doi/10.1002/2017WR020883)
973 [doi/10.1002/2017WR020883](https://onlinelibrary.wiley.com/doi/10.1002/2017WR020883) doi: 10.1002/2017WR020883
- 974 Lamb, M. P., Brun, F., & Fuller, B. M. (2017b, March). Hydrodynamics of steep
975 streams with planar coarse-grained beds: Turbulence, flow resistance, and
976 implications for sediment transport. *Water Resources Research*, 53(3), 2240–
977 2263. Retrieved 2021-11-12, from [https://onlinelibrary.wiley.com/doi/](https://onlinelibrary.wiley.com/doi/10.1002/2016WR019579)
978 [10.1002/2016WR019579](https://onlinelibrary.wiley.com/doi/10.1002/2016WR019579) doi: 10.1002/2016WR019579
- 979 Lamb, M. P., Dietrich, W. E., & Venditti, J. G. (2008, May). Is the criti-
980 cal Shields stress for incipient sediment motion dependent on channel-bed
981 slope? *Journal of Geophysical Research*, 113(F2), F02008. Retrieved
982 2021-11-12, from <http://doi.wiley.com/10.1029/2007JF000831> doi:
983 10.1029/2007JF000831
- 984 Lee, H., & Balachandar, S. (2012, March). Critical shear stress for incipient motion
985 of a particle on a rough bed: CRITICAL STRESS FOR INCIPIENT MO-
986

- 987 TION. *Journal of Geophysical Research: Earth Surface*, 117(F1), n/a–n/a.
 988 Retrieved 2023-02-03, from <http://doi.wiley.com/10.1029/2011JF002208>
 989 doi: 10.1029/2011JF002208
- 990 Lee, H., & Balachandar, S. (2017, January). Effects of wall roughness on
 991 drag and lift forces of a particle at finite Reynolds number. *International*
 992 *Journal of Multiphase Flow*, 88, 116–132. Retrieved 2023-05-06, from
 993 <https://linkinghub.elsevier.com/retrieve/pii/S0301932216300994>
 994 doi: 10.1016/j.ijmultiphaseflow.2016.09.006
- 995 Leliavsky, S. (1955). *An introduction to fluvial hydraulics*.
- 996 Li, X., Balachandar, S., Lee, H., & Bai, B. (2019, September). Fully resolved
 997 simulations of a stationary finite-sized particle in wall turbulence over a
 998 rough bed. *Physical Review Fluids*, 4(9), 094302. Retrieved 2023-05-06,
 999 from <https://link.aps.org/doi/10.1103/PhysRevFluids.4.094302> doi:
 1000 10.1103/PhysRevFluids.4.094302
- 1001 López, R., & Barragán, J. (2008, June). Equivalent roughness of gravel-bed rivers.
 1002 *Journal of Hydraulic Engineering*, 134(6), 847–851. Retrieved 2022-04-13, from
 1003 [http://ascelibrary.org/doi/10.1061/%28ASCE%290733-9429%282008%](http://ascelibrary.org/doi/10.1061/%28ASCE%290733-9429%282008%29134%3A6%28847%29)
 1004 [29134%3A6%28847%29](http://ascelibrary.org/doi/10.1061/%28ASCE%290733-9429%282008%29134%3A6%28847%29) doi: 10.1061/(ASCE)0733-9429(2008)134:6(847)
- 1005 Maniatis, G., Hoey, T., Hodge, R., Rickenmann, D., & Badoux, A. (2020, Decem-
 1006 ber). Inertial drag and lift forces for coarse grains on rough alluvial beds
 1007 measured using in-grain accelerometers. *Earth Surface Dynamics*, 8(4), 1067–
 1008 1099. Retrieved 2022-04-13, from [https://esurf.copernicus.org/articles/](https://esurf.copernicus.org/articles/8/1067/2020/)
 1009 [8/1067/2020/](https://esurf.copernicus.org/articles/8/1067/2020/) doi: 10.5194/esurf-8-1067-2020
- 1010 Masteller, C. C., Finnegan, N. J., Turowski, J. M., Yager, E. M., & Rickenmann,
 1011 D. (2019, March). History-dependent threshold for motion revealed by con-
 1012 tinuous bedload transport measurements in a steep mountain stream. *Geo-*
 1013 *physical Research Letters*, 46(5), 2583–2591. Retrieved 2021-11-12, from
 1014 <https://onlinelibrary.wiley.com/doi/10.1029/2018GL081325> doi:
 1015 10.1029/2018GL081325
- 1016 McKenna, F., Satish, A. B., Yi, S.-R., Zsarnoczay, A., Gardner, M., & Elhaddad,
 1017 W. (2021, December). *NHERI-SimCenter/quoFEM: Version2.4.1*. Zenodo.
 1018 Retrieved 2022-02-20, from <https://zenodo.org/record/5800081> doi:
 1019 10.5281/ZENODO.5800081
- 1020 Metropolis, N., & Ulam, S. (1949). The Monte Carlo Method. *Journal of the Ameri-*
 1021 *can statistical association*, 44(247), 335–341.
- 1022 Meyer-Peter, & Müller. (1948). Formulas for bed-load transport. *IAHSR 2nd meet-*
 1023 *ing, Stockholm, appendix 2*.
- 1024 Mueller, E. R., Pitlick, J., & Nelson, J. M. (2005, April). Variation in the refer-
 1025 ence Shields stress for bed load transport in gravel-bed streams and rivers.
 1026 *Water Resources Research*, 41(4). Retrieved 2022-02-20, from [http://](http://doi.wiley.com/10.1029/2004WR003692)
 1027 doi.wiley.com/10.1029/2004WR003692 doi: 10.1029/2004WR003692
- 1028 Paintal, A. S. (1971, January). Concept of critical shear stress in loose bound-
 1029 ary open channels. *Journal of Hydraulic Research*, 9(1), 91–113. Retrieved
 1030 2021-11-12, from [https://www.tandfonline.com/doi/full/10.1080/](https://www.tandfonline.com/doi/full/10.1080/00221687109500339)
 1031 [00221687109500339](https://www.tandfonline.com/doi/full/10.1080/00221687109500339) doi: 10.1080/00221687109500339
- 1032 Parker, G. (1978, November). Self-formed straight rivers with equilibrium banks
 1033 and mobile bed. Part 2. The gravel river. *Journal of Fluid Mechanics*, 89(1),
 1034 127–146. Retrieved 2023-03-28, from [https://www.cambridge.org/core/](https://www.cambridge.org/core/product/identifier/S0022112078002505/type/journal_article)
 1035 [product/identifier/S0022112078002505/type/journal_article](https://www.cambridge.org/core/product/identifier/S0022112078002505/type/journal_article) doi:
 1036 10.1017/S0022112078002505
- 1037 Parker, G. (1991, February). Selective Sorting and Abrasion of River Gravel.
 1038 II: Applications. *Journal of Hydraulic Engineering*, 117(2), 150–171.
 1039 Retrieved 2023-02-20, from [https://ascelibrary.org/doi/10.1061/](https://ascelibrary.org/doi/10.1061/%28ASCE%290733-9429%281991%29117%3A2%28150%29)
 1040 [%28ASCE%290733-9429%281991%29117%3A2%28150%29](https://ascelibrary.org/doi/10.1061/%28ASCE%290733-9429%281991%29117%3A2%28150%29) doi: 10.1061/
 1041 [%28ASCE%290733-9429\(1991\)117:2\(150\)](https://ascelibrary.org/doi/10.1061/%28ASCE%290733-9429%281991%29117%3A2%28150%29)

- 1042 Perron, J. T., Lamb, M. P., Koven, C. D., Fung, I. Y., Yager, E., & Ádámkóvics,
 1043 M. (2006, November). Valley formation and methane precipitation rates
 1044 on Titan. *Journal of Geophysical Research*, *111*(E11), E11001. Retrieved
 1045 2021-11-12, from <http://doi.wiley.com/10.1029/2005JE002602> doi:
 1046 10.1029/2005JE002602
- 1047 Pfeiffer, A. M., Finnegan, N. J., & Willenbring, J. K. (2017, March). Sediment
 1048 supply controls equilibrium channel geometry in gravel rivers. *Proceedings of*
 1049 *the National Academy of Sciences*, *114*(13), 3346–3351. Retrieved 2023-02-20,
 1050 from <https://pnas.org/doi/full/10.1073/pnas.1612907114> doi: 10.1073/
 1051 pnas.1612907114
- 1052 Phillips, C. B., Masteller, C. C., Slater, L. J., Dunne, K. B. J., Francalanci, S., Lan-
 1053 zoni, S., ... Jerolmack, D. J. (2022, May). Threshold constraints on the
 1054 size, shape and stability of alluvial rivers. *Nature Reviews Earth & Environ-*
 1055 *ment*, *3*(6), 406–419. Retrieved 2023-02-20, from [https://www.nature.com/](https://www.nature.com/articles/s43017-022-00282-z)
 1056 [articles/s43017-022-00282-z](https://www.nature.com/articles/s43017-022-00282-z) doi: 10.1038/s43017-022-00282-z
- 1057 Pierce, J. K., Hassan, M. A., & Ferreira, R. M. L. (2022, August). Probabilis-
 1058 tic description of bedload fluxes from the aggregate dynamics of individ-
 1059 ual grains. *Earth Surface Dynamics*, *10*(4), 817–832. Retrieved 2023-07-
 1060 29, from <https://esurf.copernicus.org/articles/10/817/2022/> doi:
 1061 10.5194/esurf-10-817-2022
- 1062 Prancevic, J. P., & Lamb, M. P. (2015, February). Particle friction angles in
 1063 steep mountain channels: Friction angles in mountain channels. *Jour-*
 1064 *nal of Geophysical Research: Earth Surface*, *120*(2), 242–259. Retrieved
 1065 2021-11-12, from <http://doi.wiley.com/10.1002/2014JF003286> doi:
 1066 10.1002/2014JF003286
- 1067 Prancevic, J. P., Lamb, M. P., & Fuller, B. M. (2014, March). Incipient sediment
 1068 motion across the river to debris-flow transition. *Geology*, *42*(3), 191–194.
 1069 Retrieved 2022-02-20, from [http://pubs.geoscienceworld.org/geology/](http://pubs.geoscienceworld.org/geology/article/42/3/191/131486/Incipient-sediment-motion-across-the-river-to)
 1070 [article/42/3/191/131486/Incipient-sediment-motion-across-the-river](http://pubs.geoscienceworld.org/geology/article/42/3/191/131486/Incipient-sediment-motion-across-the-river-to)
 1071 [-to](http://pubs.geoscienceworld.org/geology/article/42/3/191/131486/Incipient-sediment-motion-across-the-river-to) doi: 10.1130/G34927.1
- 1072 Páhtz, T., Clark, A. H., Valyrakis, M., & Durán, O. (2020, March). The Physics of
 1073 Sediment Transport Initiation, Cessation, and Entrainment Across Aeolian and
 1074 Fluvial Environments. *Reviews of Geophysics*, *58*(1). Retrieved 2023-01-31,
 1075 from <https://onlinelibrary.wiley.com/doi/abs/10.1029/2019RG000679>
 1076 doi: 10.1029/2019RG000679
- 1077 Recking, A. (2009, April). Theoretical development on the effects of chang-
 1078 ing flow hydraulics on incipient bed load motion: INCIPIENT MOTION
 1079 CONDITIONS. *Water Resources Research*, *45*(4). Retrieved 2023-03-
 1080 03, from <http://doi.wiley.com/10.1029/2008WR006826> doi: 10.1029/
 1081 2008WR006826
- 1082 Riebe, C. S., Sklar, L. S., Overstreet, B. T., & Wooster, J. K. (2014, February).
 1083 Optimal reproduction in salmon spawning substrates linked to grain size
 1084 and fish length: OPTIMAL REPRODUCTION IN SALMON SPAWNING
 1085 SUBSTRATES. *Water Resources Research*, *50*(2), 898–918. Retrieved
 1086 2023-02-20, from <http://doi.wiley.com/10.1002/2013WR014231> doi:
 1087 10.1002/2013WR014231
- 1088 Scheingross, J. S., Winchell, E. W., Lamb, M. P., & Dietrich, W. E. (2013,
 1089 June). Influence of bed patchiness, slope, grain hiding, and form drag
 1090 on gravel mobilization in very steep streams. *Journal of Geophysical Re-*
 1091 *search: Earth Surface*, *118*(2), 982–1001. Retrieved 2022-02-20, from
 1092 <http://doi.wiley.com/10.1002/jgrf.20067> doi: 10.1002/jgrf.20067
- 1093 Schmeeckle, M. W., Nelson, J. M., & Shreve, R. L. (2007, April). Forces on sta-
 1094 tionary particles in near-bed turbulent flows. *Journal of Geophysical Re-*
 1095 *search*, *112*(F2), F02003. Retrieved 2021-11-12, from [http://doi.wiley.com/](http://doi.wiley.com/10.1029/2006JF000536)
 1096 [10.1029/2006JF000536](http://doi.wiley.com/10.1029/2006JF000536) doi: 10.1029/2006JF000536

- 1097 Seminara, G., Solari, L., & Parker, G. (2002, November). Bed load at low Shields
1098 stress on arbitrarily sloping beds: Failure of the Bagnold hypothesis: FAIL-
1099 URE OF THE BAGNOLD HYPOTHESIS. *Water Resources Research*,
1100 38(11), 31–1–31–16. Retrieved 2023-07-29, from [http://doi.wiley.com/](http://doi.wiley.com/10.1029/2001WR000681)
1101 10.1029/2001WR000681 doi: 10.1029/2001WR000681
- 1102 Shields, A. (1936). Application of similarity principles and turbulence research to
1103 bed-load movement.
- 1104 Shvidchenko, A. B., Pender, G., & Hoey, T. B. (2001, August). Critical shear
1105 stress for incipient motion of sand/gravel streambeds. *Water Resources Re-*
1106 *search*, 37(8), 2273–2283. Retrieved 2022-02-20, from [http://doi.wiley.com/](http://doi.wiley.com/10.1029/2000WR000036)
1107 10.1029/2000WR000036 doi: 10.1029/2000WR000036
- 1108 Smart, G., & Habersack, H. (2007, September). Pressure fluctuations and gravel
1109 entrainment in rivers. *Journal of Hydraulic Research*, 45(5), 661–673. Re-
1110 trieved 2023-03-08, from [https://www.tandfonline.com/doi/full/10.1080/](https://www.tandfonline.com/doi/full/10.1080/00221686.2007.9521802)
1111 00221686.2007.9521802 doi: 10.1080/00221686.2007.9521802
- 1112 Sobol, I. (2001, February). Global sensitivity indices for nonlinear mathemat-
1113 ical models and their Monte Carlo estimates. *Mathematics and Com-*
1114 *puters in Simulation*, 55(1-3), 271–280. Retrieved 2022-02-20, from
1115 <https://linkinghub.elsevier.com/retrieve/pii/S0378475400002706>
1116 doi: 10.1016/S0378-4754(00)00270-6
- 1117 Strand, R. (1973). *Sedimentation, in U.S. Bureau of Reclamation, Design of small*
1118 *dams*. Washington, D. C., U.S. Government Printing Office.
- 1119 Turowski, J. M. (2010, August). Probability distributions of bed load transport
1120 rates: A new derivation and comparison with field data: PROBABILITY
1121 DISTRIBUTIONS OF BEDLOAD TRANSPORT. *Water Resources Re-*
1122 *search*, 46(8). Retrieved 2023-07-29, from [http://doi.wiley.com/10.1029/](http://doi.wiley.com/10.1029/2009WR008488)
1123 2009WR008488 doi: 10.1029/2009WR008488
- 1124 Vollmer, S., & Kleinhans, M. G. (2007, May). Predicting incipient motion, in-
1125 cluding the effect of turbulent pressure fluctuations in the bed: PREDICT-
1126 ING INCIPIENT MOTION. *Water Resources Research*, 43(5). Retrieved
1127 2023-03-03, from <http://doi.wiley.com/10.1029/2006WR004919> doi:
1128 10.1029/2006WR004919
- 1129 Whitaker, A. C., & Potts, D. F. (2007, July). Analysis of flow competence in an
1130 alluvial gravel bed stream, Dupuyer Creek, Montana. *Water Resources Re-*
1131 *search*, 43(7). Retrieved 2022-02-20, from [http://doi.wiley.com/10.1029/](http://doi.wiley.com/10.1029/2006WR005289)
1132 2006WR005289 doi: 10.1029/2006WR005289
- 1133 Wiberg, P. L., & Smith, J. D. (1987, August). Calculations of the critical shear
1134 stress for motion of uniform and heterogeneous sediments. *Water Re-*
1135 *sources Research*, 23(8), 1471–1480. Retrieved 2021-11-12, from [http://](http://doi.wiley.com/10.1029/WR023i008p01471)
1136 doi.wiley.com/10.1029/WR023i008p01471 doi: 10.1029/WR023i008p01471
- 1137 Wickert, A. D., & Schildgen, T. F. (2019, January). Long-profile evolution of
1138 transport-limited gravel-bed rivers. *Earth Surface Dynamics*, 7(1), 17–43.
1139 Retrieved 2023-02-23, from [https://esurf.copernicus.org/articles/7/17/](https://esurf.copernicus.org/articles/7/17/2019/)
1140 2019/ doi: 10.5194/esurf-7-17-2019
- 1141 Williams, R. M. E., Grotzinger, J. P., Dietrich, W. E., ..., & Moores, J. E. (2013,
1142 May). Martian Fluvial Conglomerates at Gale Crater. *Science*, 340(6136),
1143 1068–1072. Retrieved from [https://www.science.org/doi/10.1126/](https://www.science.org/doi/10.1126/science.1237317)
1144 [science.1237317](https://www.science.org/doi/10.1126/science.1237317) doi: 10.1126/science.1237317
- 1145 Wohl, E., Bledsoe, B. P., Jacobson, R. B., Poff, N. L., Rathburn, S. L., Walters,
1146 D. M., & Wilcox, A. C. (2015, April). The Natural Sediment Regime in
1147 Rivers: Broadening the Foundation for Ecosystem Management. *BioScience*,
1148 65(4), 358–371. Retrieved 2023-02-20, from [http://academic.oup.com/](http://academic.oup.com/bioscience/article/65/4/358/254680/The-Natural-Sediment-Regime-in-Rivers-Broadening)
1149 [bioscience/article/65/4/358/254680/The-Natural-Sediment-Regime-in-](http://academic.oup.com/bioscience/article/65/4/358/254680/The-Natural-Sediment-Regime-in-Rivers-Broadening)
1150 [-Rivers-Broadening](http://academic.oup.com/bioscience/article/65/4/358/254680/The-Natural-Sediment-Regime-in-Rivers-Broadening) doi: 10.1093/biosci/biv002
- 1151 Wong, M., & Parker, G. (2006, November). Reanalysis and Correction of Bed-Load

- 1152 Relation of Meyer-Peter and Müller Using Their Own Database. *Journal*
1153 *of Hydraulic Engineering*, 132(11), 1159–1168. Retrieved 2023-05-14, from
1154 [https://ascelibrary.org/doi/10.1061/%28ASCE%290733-9429%282006%](https://ascelibrary.org/doi/10.1061/%28ASCE%290733-9429%282006%29132%3A11%281159%29)
1155 [29132%3A11%281159%29](https://ascelibrary.org/doi/10.1061/%28ASCE%290733-9429%282006%29132%3A11%281159%29) doi: 10.1061/(ASCE)0733-9429(2006)132:11(1159)
- 1156 Wu, F.-C., & Shih, W.-R. (2012, September). Entrainment of sediment particles
1157 by retrograde vortices: Test of hypothesis using near-particle observations.
1158 *Journal of Geophysical Research: Earth Surface*, 117(F3), n/a–n/a. Retrieved
1159 2021-11-21, from <http://doi.wiley.com/10.1029/2011JF002242> doi:
1160 10.1029/2011JF002242
- 1161 Yager, E. M., Kirchner, J. W., & Dietrich, W. E. (2007, July). Calculating bed
1162 load transport in steep boulder bed channels: SEDIMENT TRANSPORT
1163 IN STEEP CHANNELS. *Water Resources Research*, 43(7). Retrieved
1164 2023-02-20, from <http://doi.wiley.com/10.1029/2006WR005432> doi:
1165 10.1029/2006WR005432
- 1166 Yager, E. M., Schmeeckle, M. W., & Badoux, A. (2018, December). Resistance
1167 is not futile: Grain resistance controls on observed critical Shields stress
1168 variations. *Journal of Geophysical Research: Earth Surface*, 123(12), 3308–
1169 3322. Retrieved 2021-11-12, from [https://onlinelibrary.wiley.com/doi/](https://onlinelibrary.wiley.com/doi/10.1029/2018JF004817)
1170 [10.1029/2018JF004817](https://onlinelibrary.wiley.com/doi/10.1029/2018JF004817) doi: 10.1029/2018JF004817
- 1171 Yager, E. M., Venditti, J. G., Smith, H. J., & Schmeeckle, M. W. (2018, Decem-
1172 ber). The trouble with shear stress. *Geomorphology*, 323, 41–50. Re-
1173 trieved 2023-02-03, from [https://linkinghub.elsevier.com/retrieve/](https://linkinghub.elsevier.com/retrieve/pii/S0169555X18303659)
1174 [pii/S0169555X18303659](https://linkinghub.elsevier.com/retrieve/pii/S0169555X18303659) doi: 10.1016/j.geomorph.2018.09.008